Reactive transport modeling of glass alteration in a fractured vitrified nuclear glass canister: From upscaling to experimental validation

Maria Repina, Frederic Bouyer, Vincent Lagneau

Version of Record: https://www.sciencedirect.com/science/article/pii/S0022311519304258
Manuscript_61db34bf20e65aa013e9126199d12408

Reactive transport modeling of glass alteration in a fractured vitrified nuclear glass canister: from upscaling to experimental validation

Maria Repina[a,b], Frédéric Bouyer[a,1], Vincent Lagneau[b]

[a] CEA, DEN, MAR, DE2D, SEVT, LCLT Marcoule, F 30207 BAGNOLS SUR CEZE Cedex, France

[b] MINES ParisTech - PSL Research University, Centre de Géosciences 35, Rue Saint-Honoré F 77305 FONTAINEBLEAU Cedex, France

Abstract

Performance assessment of geological nuclear waste repositories entails modelling of the long-term evolution of the aqueous alterations of the fractured nuclear glass block, because the time scales under consideration are of several thousands of years and hence beyond the range of any direct experimental perspectives. In this study, our objective is to bridge the gap between the reservoir-scale flow and transport simulations and the micron-scale modeling of the glass-water interfacial processes by providing quantitative evaluation of the aqueous alteration of glass at the block scale. In particular, calculations of the equivalent diffusive, hydraulic, and alteration kinetics properties and reactive transport simulations are discussed. Prior to performing reactive transport modeling at the scale of the glass canister, the preferred upscaling techniques were first applied to a synthetic fracture network system with ends to compare the results of the borosilicate glass alteration with the discrete fracture modeling and the equivalent porous medium approach. The evolution of the altered glass obtained from reactive transport modeling applied to several realizations of the equivalent fracture network tessellation was compared to the experimental data of the aqueous alteration test of a nonradioactive full-scale SON68 glass canister. The proposed model agrees with the experimental data and offers, for the first time, an opportunity to better understand the impact of fracturing as the convection due to the radioactivity acting as a heating source on the corrosion of nuclear glass.

Keywords

Nuclear glass corrosion, fracture network, glass alteration rate, reactive transport modeling, upscaling, equivalent continuum, kinetic regimes.

Introduction

The vitrification of radioactive waste has been considered as a reliable method to condition high-level long-lived nuclear fission products in geological disposal facilities on time scales of up to millions of years. This process involves calcination of the liquid fission product solutions followed by melting at around 1100 °C in an induction-heated metallic vessel, where the glass frit and the calcinated fission product solution are mixed before being poured into a metallic container. During cooling and solidification of the glass, the increase of tensile stresses resulting from the mechanical

[1] Corresponding author CEA, DEN, MAR, DE2D, SEVT, LCLT Marcoule, F 30207 BAGNOLS SUR CEZE Cedex, France. E-mail address: frederic.bouyer@cea.fr (BOUYER Frederic)

equilibrium between the shrinking internal liquid and the solidified external glass causes the development of a network of fractures.

ANDRA, the French national operator for the management of nuclear waste, and numerous academic or national operators worldwide have been carrying out research concerning the feasibility of geological waste disposal. In consideration of the results of several decades of research, the French Parliament opted for deep geological disposal and asked ANDRA to design Cigéo (Centre industriel de stockage géologique) – a deep geological disposal facility for radioactive waste. According to the disposal scenario proposed by ANDRA, the packages of vitrified fractured glass containing high-level long-lived radioactive waste (HLLLW) would be stored in disposal cells in a repository built with Callovo-Oxfordian (COx) clay, located 500 m beneath the Earth surface in Meuse/Haute-Marne, France. With the current concept (which is still in development), these cells would be blind micro-tunnels, 0.7 m in diameter and of 100–150 m total length (Figure 1a). A steel lining is intended to facilitate the placement of packages during the operational phase (and their removal for possible recovery). Finally, a filler material would be injected between the liner and the host rock to enhance mechanical strength and reduce corrosion. The glass canisters made of vitrified glass contained in 53–65 mm thick steel overpacks (Figure 1b) would be positioned separately from one another, such that heat production in the cell is compatible with thermo-hydro-mechanical targets [1].

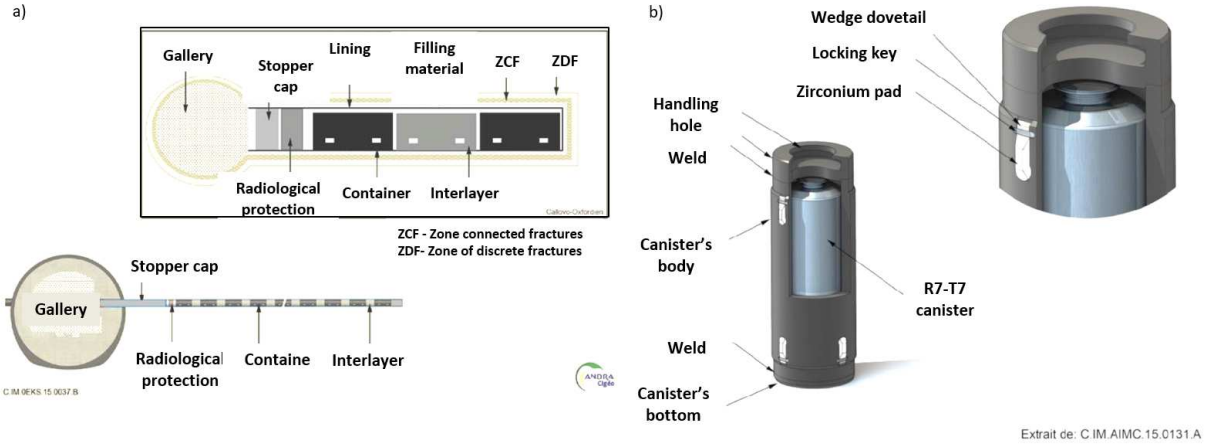

Figure 1 a) Schematic diagram of the high activity HA cell; b) Illustration of an HA storage container for vitrified nuclear waste, primary package type R7T7. High-level long-lived waste disposal gallery in operating configuration. Obtained from [1].

As mentioned above, the cooling down stage creates numerous fractures in the vitrified glass packages. The fracture network increases the reactive surface areas and creates water pathways within the glass. After re-saturation of the vicinity of the cell, and the eventual corrosion of the canister, water will come into contact with the glass. The water-glass interaction must therefore be studied, both in terms of glass alteration and release-rate of radionuclides.

Despite the advancements made in studies of solute transport and flow of ground water in fractures at the mega-scale [2-5] and discoveries achieved in the domain of borosilicate glass aqueous alteration [6,7] at the micro-scale, the reactive transport modeling applied to a scale of one block of fractured borosilicate glass has not been performed to date, to the best of our knowledge.

Although the evolution of reactive transport modeling (RTM) codes is impressive, RTM applied to fractured media of a glass block remains challenging. Particularly, the coupling of the geochemistry of

borosilicate glass dissolution with physical flow and transport phenomena within a discrete fracture network is too CPU-intensive. Hence, to study nuclear glass degradation at the scale of the industrial vitrified glass canister, an equivalent fracture network model was constructed, and its hydraulic, diffusive and kinetics controlling parameters were determined.

This study is a further development of our previous research [8], where the authors presented an image processing-based fracture network characterization workflow elaborated for RTM application to a block of vitrified nuclear glass. The workflow was devised in the following steps: (i) characterization of a glass block fracture network, (ii) establishment of a link between a physical parameter representing an internal state of glass structural relaxation and an internal structure of the block fracture network, and (iii) generation of multiple realizations of fracture networks by considering the variability of fracture network parameters such as fracture distribution and aperture. Based on mapped fracture distribution and aperture, the present paper presents an upscaling workflow and subsequent RTM application as follows: computation of the equivalent hydraulic, diffusive, and glass degradation kinetics- governing parameters, verification of the proposed techniques, their application to several realizations of fracture networks, and reactive transport modeling. The construction of the equivalent continuum model was initiated to overcome the problem of the complexity of the fracture network discrete representations and, as a consequence, to be able to perform RTM at the scale of the industrial glass canister.

RTM was conducted by the HYTEC code [9,10]. The kinetics of the international simple glass (ISG) aqueous alteration [7], including the passivation effect of dense gel formation, is represented using the Glass Reactivity with allowance for the Alteration Layer (GRAAL) model. ISG glass aqueous alteration was studied under the assumption of full saturation with water in pH conditions preventing alteration resumption. The methodology was tested over synthetic discrete fracture networks, and finally an application is performed at the block scale to simulate a long-term aqueous alteration experiment of a non-radioactive proxy canister.

1 Material

1.1 Aqueous alteration experiment of a nonradioactive full-scale SON68 glass block

French Alternative Energies and Atomic Energy Commission CEA performed an aqueous alteration experiment on a non-radioactive full-scale inert nuclear glass canister [11]. The experiment was conducted in the ALISE (Appareillage de Lixiviation Statique Électrique) unit built in Marcoule. The objective of this experiment was to produce a set of data on the long-term (seven years) aqueous alteration of an industrial-scale vitrified glass canister under static conditions with a moderate amount of water in contact with the glass (about 35 L for one block of 400 kg). The general schematic of the installation is depicted in Figure 2.

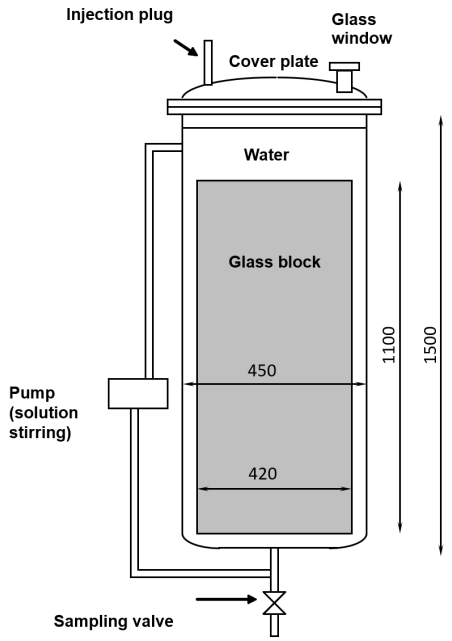

Figure 2 General view of the ALISE unit. Dimensions indicated on the sketch are in mm. Modified from [11].

An industrial-scale block of inert nuclear glass was fabricated in a cold crucible in two stages. This 400 kg block was made in a perforated stainless steel basket with 10 mm diameter holes to facilitate water access during the experiment.

Soon after the fabrication of the block, it was placed into the ALISE unit. It remained there for 2718 days (7.5 years). The initial temperature was set to 106 ± 1 °C. The heating system consisted of two classical heating collars. Three thermocouples monitored the evolution of the temperature inside the ALISE unit. The initial volume of water in the reactor was 34.7 liters. In total, over the course of the test, over a hundred samples were collected and analyzed by ICP/AES for Si, B and some other elements. Prior to each sample collection, the solution was homogenized for thirty minutes using closed-loop pumping.

It should be noted that there were some interventions. First, after 1840 d from the beginning of the test, the reactor was opened to estimate the amount of the evaporated solution[2]. Second, after 2030 d, eight liters of a synthetic solution was added to compensate for the cumulated evaporated water. Before mixing, the solution composition was adjusted to minimize the chemical disturbance.

To characterize the glass alteration, the evolution of several parameters was monitored. First, the evolution of the boron[3] tracer element was observed. Secondly, with respect to boron concentration evolution, the alteration rate was estimated using the following equation (1):

[2] Although there was evaporation, the glass block stayed always submerged in water, there was no influence of gas phase on the glass alteration rate.

[3] Boron is considered as a tracer of glass dissolution, because it is released completely from the glass during the glass alteration process without being retained in the alteration layer [12,13].

$$alteration\ rate = \frac{C_i(t)*V}{X_i*t}, \quad (1)$$

where C_i(t) is the concentration of dissolved boron in the solution at time t, X_i is the mass fraction of boron in the glass, and V is the solution volume.

Thirdly, to characterize the reaction affinity, the evolution of the silicon concentration was traced.

1.2 Glass block section and its fracture network equivalent tessellations

The segmented image of a non-radioactive vitrified glass fracture network (Figure 3a) and three realizations of fracture network equivalent tessellations (Figure 3b–d) presented in [8] were used as the input data for this study. The glass fracture network was extracted and characterized using mathematical morphology tools. The input data necessary for the generation of multiple realizations of fracture network equivalent tessellations were obtained by conducting geostatistical modelling based on the results of image analysis and the analysis of a physical parameter indicative of glass internal structural relaxation. The parameters of the four fracture networks are indicated in Table 1.

Table 1 Fracture network parameters impacting glass alteration

Name/ Parameter	Segmented Image	Equivalent Tessellation #1	Equivalent Tessellation #2	Equivalent Tessellation #3
Average porosity	0.08	0.11	0.12	0.11
Length of fracture median axes, m	20.5	51	52.1	49.5
2D fracturing ratio	17.4	42.7	41.8	40.6
Internal fracture surface[4], m^2	26.6	67.7	66.2	66.7

[4] Calculated under the assumption that fracturing ratios in 2D and in 3D are equal.

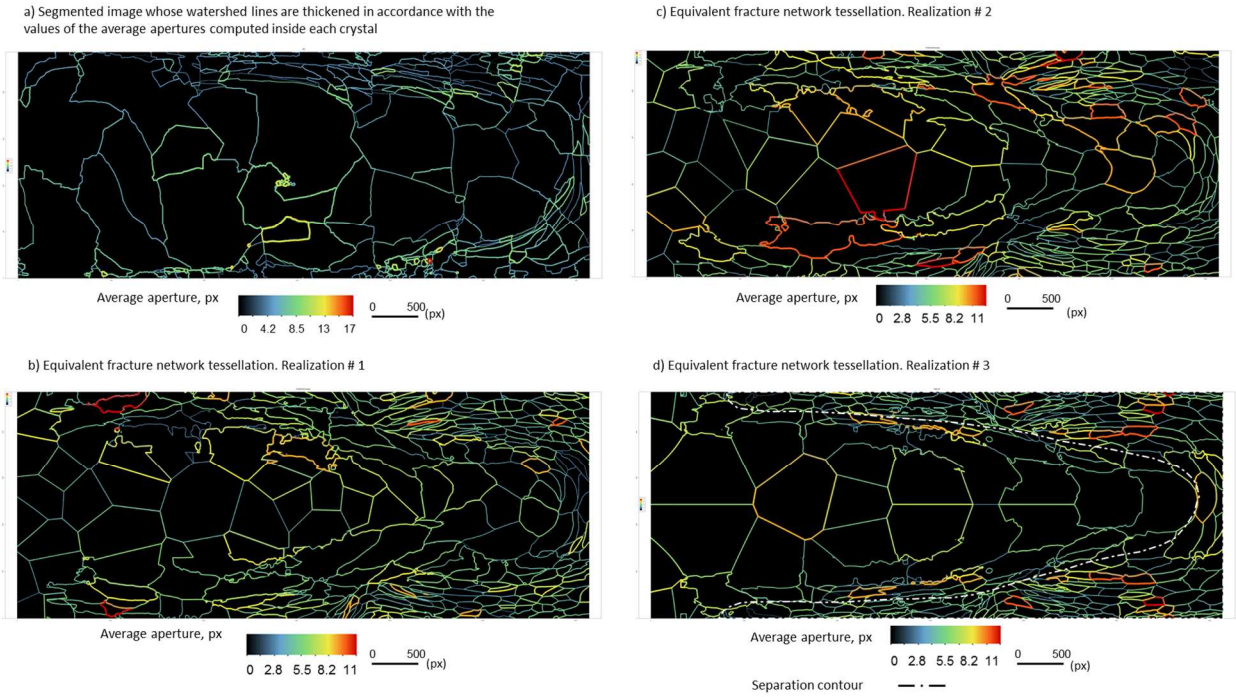

Figure 3 Input images used to calculate equivalent reactive transport parameters: segmented image of the full glass section of the canister (top left), and three equivalent tessellations used in this study. Image dimensions are 6144 px × 2430 px, with 1 px corresponding to 0.17 mm.

1.3 GRAAL geochemical model

The borosilicate nuclear glass alteration was simulated by the glass reactivity with allowance for the alteration layer (GRAAL) model [14,12,15]. The model pursues a dual objective: (i) coupling between the affinity effects in the kinetic law and the diffusion processes in the alteration layer and (ii) establishment of a precise material balance to calculate the distribution of the elements of the glass between the solution, secondary phases and a developing gel. The first hypothesis of the GRAAL model is the rate of the hydration reaction of the glass at the initial time: this phenomenon causes the elements of the glass (the alkali earth metals, boron) to pass into solution. The hydrolysis of silicon is slower and conditions the initial dissolution rate of the glass. The difference between these two kinetics leads to the formation of a dealkalized hydrated glass layer at the glass-solution interface. This layer or gel is gradually reorganized by hydrolysis / condensation phenomena and is referred to as the passivating reactive interface (PRI). Each silicon atom present in the solution stems from the dissolution of the PRI. Concurrent to its formation, this gel dissolves, given that the solution is not saturated with the elements that constitute it, namely Si, Al, Ca, and Zr. GRAAL proposes a description of the gel formed on the surface of glass by condensation and precipitation of Si, Al, Zr, and Ca. With a relatively simple formalism, the model accounts for the chemistry and solubility of the gel. It assumes that glass alteration is controlled by the PRI, consisting of glass without any mobile elements in its composition.

The transport properties of the PRI are modeled by a spatially and temporally constant diffusion coefficient for the elements of the glass. Thus, the flow of mobile elements transported through the PRI is proportional to the diffusion coefficient and inversely proportional to the thickness of the PRI. GRAAL therefore makes the assumption of a balance between the non-passivating gel and the

solution, and between the external interface of the PRI and the solution. GRAAL uses two kinetic equations for the PRI grouped in (2).

$$\frac{dx}{dt} = \mathrm{r}_1 - \mathrm{r}_2 = \frac{D_{PRI}}{\mathrm{x_{PRI}}} - v_0\left(1 - \frac{Q_{PRI}}{K_{PRI}}\right) = \frac{D_0 \times [OH^-]^{n'} \times e^{-\frac{E'_a}{RT}}}{x} - \mathrm{k}^+ \times [H^+]^{\mathrm{n}} \times e^{-\frac{E_a}{RT}} \times \left(1 - \frac{\mathrm{Q_{PRI}}}{\mathrm{K_{PRI}}}\right), \quad 2$$

This equation states that the passivating reaction interface PRI (i) is formed from the glass with a rate r_1, which is a function of its thickness $\mathrm{x_{PRI}}$ and the PRI diffusion coefficient D_{PRI}, and (ii) also dissolves with a rate r_2 according to a classical affinity law in which v_0 is the initial dissolution rate, Q_{PRI} is the ionic product and K_{PRI} is the PRI solubility product. The right hand-side of the equation is the expanded version, indicating the dependence of D_{PRI} and v_0 on pH and T, where D_0 is the interdiffusion constant, E'_a is the activation energy associated to the interdiffusion coefficient, n' is the pH-dependence factor, E_a is the apparent activation energy at the initial rate, n is the pH-dependence factor of the initial rate, k^+ is the dissolution rate of the PRI in pure water, and T is the sample temperature.

As in the study of [13], in order to limit the formation kinetics of the protective layer, *i.e.* to avoid the appearance of the infinite rate when $\mathrm{x_{PRI}} = 0$, a constant hydration rate is introduced in the definition of r_1 in (3):

$$\mathrm{r}_1 = \frac{\mathrm{D_{PRI}}}{\mathrm{x_{PRI}}} = \frac{\mathrm{r_h}}{1 + \mathrm{x_{PRI}}\frac{\mathrm{r_h}}{\mathrm{D_{PRI}}\frac{\pi}{2}}}, \quad 3$$

where $\mathrm{r_h}$ is the hydration rate, which is higher than the initial dissolution rate. This is fully compatible with the experimental observations: the dissolution rate of mobile ions is higher than the dissolution rate of silicon ions. However, due to the very low diffusion coefficient of components in nuclear glasses [16], the hydration rate governs the alteration rate only for a few seconds. The parameter is not measurable experimentally, and has almost no effect on the modeling results.

In order to perform a RTM of borosilicate glass alteration, regardless of the modeling approach used (discrete fracture network or the equivalent porous model), some parameters in the law of glass dissolution have to be specified: glass mass per solution volume C_v, glass specific surface S_{sp}, half-saturation coefficient present in the inhibition function[5] used to account for the interdiffusion rate, molar fractions of elements in the PRI, i_{PRI}, and in the glass, i_{PS}, glass molar density ρ_{PS}, and some other constants, like $\mathrm{E^a}$, k^+, n, $\mathrm{E'_a}$, $\mathrm{D_0}$, $\mathrm{n'}$ from Equation 2.

Some of the mentioned parameters, such as ρ_{PS}, k^+, i_{PRI}, i_{PS}, T, and the pH-dependence constants, $\mathrm{E^a}$ and $\mathrm{E'_a}$, are specific to the chemical properties of the glass. The others, such as C_v, S_{sp}, and the half-saturation coefficient, are controlled by the internal structure of the modeled fracture network. Depending on whether the discrete model or the equivalent porous model is applied, the calculation of these parameters changes. The exact formulas and the hypothesis constructed to compute these parameters for equivalent continuum and discrete models are discussed in Section 2.1.3 and Section 3.

[5] The inhibition function, representing a special case of the Monod equation, imposes that the interdiffusion rate is only proportional to the diffusion coefficient if half-saturation << instantaneous PRI concentration. When the PRI does not exist, the alteration rate of the glass is maximal.

In this study, the porosity update due to the precipitation of the secondary minerals in the fracture network was not considered. Indeed, in accordance with the GRAAL model, the alteration is considered isovolumetric: dissolved glass is replaced isovolumetrically by the alteration layer [17-19], such that glass alteration has no impact on fracture aperture and hydraulic conductivity.

1.4 Reactive transport modeling in HYTEC coupled code

Reactive transport simulations are performed by the HYTEC code [9]. HYTEC is a coupled chemistry-transport code that relies on the method of the separation of operators, with a sequential iterative algorithm [20,10]. The flow module is available in saturated (stationary, transitory regimes), unsaturated, and two-phase forms. It also allows for variable density flow. The variation of water densities as a function of temperatures (motor to thermo-convection) uses the Boussinesq approximation (4):

$$\frac{\rho}{\rho_0} = 1 - \alpha(T - T_0)\,, \qquad 4$$

where α is the thermal expansion coefficient, T_0 is the reference temperature at which the density is ρ_0, and T is the local temperature at which the density is ρ.

In this study, the simulations of the aqueous alteration of the borosilicate ISG glass [7] were conducted in saturated stationary and saturated transient regimes. These simulations were conducted in both diffusive and convective modes. Convection originated from an imposed temperature gradient between the lower and upper parts of the modeled glass canisters. Change in porosity and its effect on the permeability and diffusion, as a consequence of clogging or dissolution, was not considered in the simulations, in agreement with the isovolumetric phase replacement.

The grids of both discrete and equivalent models presented here were created by a three-dimensional mesh generator GMSH [21]. HYTEC uses this grid for its node-centered finite volume scheme.

The governing equations of the GRAAL model are implemented in HYTEC. The principal requirements for HYTEC to accept GRAAL equations are the availability of the Monod-type equation, the ability to use the concentration of a solid (glass) as a variable of the equation, and an adaptive time step [13]. Thus, the time step needs to be small at the beginning of the calculation when the protective layer is thin to prevent its immediate dissolution. The switch from the GRAAL model to HYTEC is performed by treating (3) as a Monod-type equation and using the general kinetic formulation [22] to describe the dissolution equation (Table 2).

Table 2 Analogy between the parameters in the GRAAL model and HYTEC code

	GRAAL model	HYTEC code
Parameter	PRI thickness $\mathrm{X_{PRI}}$	PRI concentration $\mathrm{X_{PRI}} = \frac{\mathrm{C_{PRI}}}{\rho_{\mathrm{PRI}} \mathrm{S_{sp}} \mathrm{C_v}}$
Primary solid alteration rate controlled by protective layer's thickness	$\frac{\mathrm{D_{PRI}}}{\mathrm{x_{PRI}}} = \frac{\mathrm{r_h}}{1 + \mathrm{x_{PRI}} \frac{\mathrm{r_h}}{\mathrm{D_{PRI}} \frac{\pi}{2}}}$ $\mathrm{D_{PRI}}(\mathrm{T}, \mathrm{pH}) = D_0 [OH^-]^{n'} e^{-\frac{E'_a}{RT}}$	$\mathrm{r_h} \frac{\mathrm{half-saturation}}{\mathrm{half-saturation} + \mathrm{C_{PRI}}}$ Monod type equation (inhibition) $\mathrm{half-saturation} = \frac{\mathrm{D_{PRI}} \frac{\pi}{2}}{\mathrm{r_h}} \rho_{\mathrm{PS}} \frac{\mathrm{i_{PS}}}{\mathrm{i_{PRI}}} \mathrm{S_{sp}} \mathrm{C_v}$ W term specifying the dependence of $\mathrm{D_{PRI}}$ on pH,

		for example *w-term {* *species = OH[-]* *power = -0.649* *}*
Protective layer's dissolution rate	$\mathrm{k}^{+}[H^{+}]^{\mathrm{n}}\, e^{-\frac{E_a}{RT}}\left(1-\frac{\mathrm{Q_{PRI}}}{\mathrm{K_{PRI}}}\right)$	Rate, area, Y- term specifying the dependence on the saturation state: *for example* *y-term, species = SiAl* W-term specifying the dependence on the pH, *for example* *w-term {* *species = H[+]* *power = -0.4* *}*

$\mathrm{C_{PRI}}$ is the concentration of the protective layer, $\mathrm{S_{sp}}$ is the specific surface area of the glass, and $\mathrm{C_v}$ is the concentration of the glass in the calculation cell volume. Dissolution rate parameters determined for the ISG glass were obtained from [13].

The thermodynamic data used in this study were taken from the public Common thermodynamic database for speciation models CTDP, itself derived from EQ3/6 database [23]. It was adapted at the Laboratoire d'étude du Comportement à Long Terme des matériaux de conditionnement (LCLT), CEA Marcoule, by the addition of the definition of glass composites of interest (ISG, SON68, etc.). The definition of the amorphous layers end-members and their chemical characteristics are taken from [13].

2 Methods

Determination of the equivalent properties

The reactive transport parameters considered in this study are the porosity, tortuosity, diffusion coefficient, hydraulic conductivity, and glass alteration kinetic parameters controlled by the ratio of the contact surface to the solution volume.

It has been long established that flow and transport parameters are scale dependent [24,25]. This results from the existence of multiscale structures of porous medium that induce a hierarchy, which generates the heterogeneity. Consequently, the measurement or calculation of the parameters carried out at one scale cannot be directly applied to another-scale modeling. In fact, to pass to a higher scale, *i.e.* to make model coarser, upscaling techniques need to be employed. Upscaling leads to the replacement of a heterogeneous domain by a homogeneous one that should reproduce an equivalent response with the same imposed boundary conditions. Hence, upscaling transfers parameter values from the small to the larger scale by regularizing the heterogeneities at the smaller scale [26]. Upscaling has received a lot of attention from various fields, *e.g.* reservoir engineering [27-29], hydrology [30-32], and reactive transport modeling [33,26,34].

There are numerous upscaling techniques, that are often sorted in several groups: most notably volume averaging [35], homogenization [36], renormalization [37,38], ensemble averaging [39], and continuous-time random walk [40]. Despite the fact that these techniques have a lot of differences,

their goal is basically the same: to relate the microscopic-scale structures and properties to the associated effective, or sometimes termed equivalent parameters [41] considered in the macroscopic transport and flow equations.

In this study, we deal with the construction of an equivalent continuum model, meaning that the issue of the upscaling of permeability and diffusion is tackled. Although the construction of the equivalent continuum model is delicate because of the problematic choice of the representative elementary volume (REV) due to the disparate character of fracture density inside a glass canister, this model is able to provide the first estimate of the impact of fractures on nuclear glass aqueous corrosion in the geologic repository environment. Moreover, upscaling is also necessary for the geochemical description of glass alteration: the geochemical model of the borosilicate glass corrosion [12] is entirely adopted in the equivalent continuum modeling.

In the next sections we address the calculation of the maps of porosity, permeability, and effective diffusion and furthermore, we focus on the calculation of the equivalent glass corrosion kinetic parameters.

2.1 Equivalent permeability

The objective here is to calculate the maps of equivalent permeability, which would result in the same total flow of single-phase fluid through the coarse, homogeneous mesh as that obtained from the geometric description of the fracture network. It should be noted, that although there is some evidence that under geo-repository conditions a two-phase flow would take place due to the liberation of hydrogen as a result of the steel corrosion and radiolysis, in this research we considered that both flow and geochemical alteration happen under a water saturated condition.

The equivalent permeability was calculated by the simplified renormalization technique proposed in [42,43]. As in all renormalization techniques, the studied parameter is considered at several levels. At each stage, the map of the considered effective parameter is computed by renormalizing the map of the parameter at the preceding step. The idea of the simplified normalization method is to first assemble cells in groups of N × N cells at each step of the calculation, second, for each assembled group to calculate either the harmonic mean followed by the arithmetic mean or the arithmetic mean followed by the harmonic mean depending on the direction of the calculation with respect to the flow direction, third, at the end of stage before passing to the next level, to compute the geometric mean of the two previous results. The procedure is considered completed when the size of the coarse mesh is reached.

The fracture permeability on the initial map of fracture apertures was obtained using the parallel-plate model. Values of fracture permeability were computed using the relationship derived from the Hagen-Poiseuille solution of the Navier-Stokes equation, which relates the intrinsic fracture permeability to its aperture as defined in (5):

$$K_f = {a^2}/{12}, \qquad 5$$

where a is the fracture aperture.

Matrix permeability was taken as equal to 10^{-18} m^2 with reference to the study on thermo-mechanical cracking effects on elastic wave velocities, mechanical strength, and permeability under pressure [44].

2.2 Equivalent diffusion

The efficiency of the random walk method applied to solve the diffusion problem is largely recognized [45]. In the random walk techniques, the determination of diffusivity of the media relies on the Einstein relation [46], relating the mean square displacement to the effective diffusion coefficient (6):

$$R^2(t) = \langle (r(t) - r(t=0))^2 \rangle = 2dD(t)t, \qquad 6$$

where d is the system dimension (1d, 2d or 3d), D(t) is the diffusion coefficient, r(t) particle position at t, and r(t=0) is the particle position at t=0. It should be noted, that the square displacement is averaged for all particles.

The self-diffusion coefficient of molecules in a limitless bulk media is independent of time. It is only controlled by the type of molecules and by the fluid in which molecules diffuse. However, this diffusion coefficient becomes time-dependent when calculated in heterogeneous porous media.

Multiple studies have shown [47-50] that in the case of heterogeneous media, the convergence of the diffusion coefficient D(t) to its asymptotic value of effective diffusion (D_{eff}) is reached once the squared displacement $R^2(t)$ exceeds the permeability correlation length. In other words, to obtain the information about the true molecule trajectories encoded in the diffusion coefficient, it is necessary to allow the molecules to discover the whole domain. The short-time behavior of the mean squared displacement *vs.* time determines the surface-volume ratio of the porous media, because at short time scales, the molecules do not sense heterogeneities of the media [49,51].

In this study, we attempt to evaluate the tortuosity and the effective diffusion coefficient from the images of fracture networks shown in Figures 3 and 4a. This is carried out by modeling a 2D random walk in the percolating fracture space as follows.

1. N_{part} independent particles are placed randomly in each cell of the output grid.
2. At each iteration Δt, they can move to 4 neighboring positions (–X, +X, –Y, +Y) inside the fracture network, over a distance equal to 1. In the case where they encounter the glass, the displacement is not incremented. If particles leave the cell, they continue their paths in the fracture medium created by a mirror (toroidal) reflection.
3. Euclidean distance and directional displacements between the initial and the final locations for each particle are calculated and then averaged for all particles.
4. The regression of the average of the squared distances as a function of the iteration is verified for linearity, and the slope of the linear regression is recorded.

In general, in the case of the particle diffusion in free limitless space, the slope of the mean square displacement (msd) *vs.* time is equal to 1, whereas for the diffusion in fractured systems when motion is restricted by the glass matrix, the slope is less than 1. It reflects the impact of geometrical features on the particle diffusion, such as tortuosity of the porous media. To be precise, the tortuosity that determines the ratio of the effective average path of fluid particles to the corresponding straight and shortest distance along the direction of the flux is equal to the inverse of the slope according to the equations (7–8) given for the directional diffusion tortuosity.

$$\tau_{D_x} = \frac{1}{2}\left[\lim_{t\to\infty} \frac{d\langle (x(t)-x(t=0))^2\rangle}{dt}\right]^{-1}, \quad 7$$

$$\tau_{D_y} = \frac{1}{2}\left[\lim_{t\to\infty} \frac{d\langle (y(t)-y(t=0))^2\rangle}{dt}\right]^{-1}, \quad 8$$

where d/dt is the derivative sign. t, x and y are dimensionless time and coordinates.

Subsequently, in accordance with the equations (9–10), the directional coefficients of effective diffusion and the average diffusion coefficient are calculated.

$$D_x^e = \phi D_w \frac{1}{\tau_{D_x}}, \quad 9$$

$$D_y^e = \phi D_w \frac{1}{\tau_{D_y}}, \quad 10$$

where ϕ is the porosity of the fracture medium, and D_w is the water self-diffusion coefficient.

Meanwhile, it should be mentioned that it is not recommended to apply the described procedure to a low-density fracture network. In fact, in low density fractured media where fractures are not branched, it is difficult to record the average diffusion coefficient because particles move for a long time only in one direction before discovering the next fracture ramification. For this reason, at the scale of glass canister, the coefficient of effective diffusion for the inner part of the fracture network is calculated with the assumption that $\tau_{D_x} = \tau_{D_y}$= 1. The example of one block partitioning into inner and outer parts is shown in Figure 3d. The separation contour corresponds to the maximum gradient of the map of the arrival times of the solidification front.

Prior to application to a fracture network at the scale of the glass canister, the method is verified by comparing random walk on a discrete fracture network and on the calculated equivalent porous medium. Synthetic fracture networks were created, and the fracture density was chosen in accordance with the target fracture network in the glass canister and the desired upscaling. The evolution of particle concentration (N_{part} in a cell/N_{part}) in each cell of the output grid is recorded and analyzed, in order to investigate the resemblance of particle movement in the synthetic fracture medium and its equivalent porous system. The procedure is the following.

1. For the image in Figure 4a, the limiting slopes of the mean square displacement in X and Y directions ($slope_x^{cell(i)}$, $slope_y^{cell(i)}$) are calculated in accordance with the procedure explained above.
2. The resulting values are assigned to the elementary displacements $\Delta x^{cell(i)} = slope_x^{cell(i)}$, $\Delta y^{cell(i)} = slope_y^{cell(i)}$ that particles can effectuate in X and Y directions in each cell during their walk in the equivalent porous system.
3. The equivalent porous system is created by taking into account the porosity of the discrete fracture medium, *i.e.* the dimensions of each cell of the equivalent porous grid are calculated as defined in (11):

$$\mathrm{dx}_{cell} = {}^{a}/_{N_x} \times \sqrt{\Phi_{cell}} \text{ and } \mathrm{dy}_{cell} = {}^{b}/_{N_y} \times \sqrt{\Phi_{cell}}, \quad 11$$

where a and b are the dimensions of the fracture network image, N_x and N_y depict the number of cells in x and y directions, and Φ_{cell} is the porosity of the cell where particles are counted.

4. In the case of the discrete fracture network, N particles are placed at the point with the smallest abscissa and ordinate values of the fracture network. They could travel to four neighboring positions inside the fractures during T iterations, with the maximum Δx and Δy elementary displacement being equal to 1.
5. As for the equivalent porous media, the same number N of particles were placed at the (0,0) point. They could travel to four neighboring positions inside the fractures during T iterations. Their elementary displacements were as specified at stage 2. The particles were not allowed to leave the media: they were reflected by the boundaries, and their displacements were incremented in a normal way.
6. At each iteration, the particles present in each cell were calculated and divided by the total number of the particles.

2.3 Equivalent glass corrosion kinetic governing parameters

Since the glass aqueous alteration is controlled by the product of the glass mass per solution volume by the glass specific surface ($C_v \times S_{sp}$), which is determined by the internal structure of the fracture network, the goal of this step is to build the grids of the C_v, S_{sp}, half-saturation coefficient according to the equations (12–14):

$$C_v = \frac{M_g}{V_s} = \frac{(1-\Phi)\rho}{\Phi}, \quad 12$$

$$S_{sp} = \frac{2Lc}{M_g} = \frac{2L}{ab(1-\Phi)\rho}, \quad 13$$

$$\text{half saturation} = \lambda \frac{D_{PRI}}{r_h} \rho_{PS} \frac{i_{PS}}{i_{PRI}} \times \frac{1}{\Phi} \times \frac{2L}{ab} = D_o [OH^-]^n \exp(-\frac{E_a}{RT}) \times \frac{\lambda}{r_h} \rho_{PS} \frac{i_{PS}}{i_{PRI}} \times \frac{1}{\Phi} \times \frac{2L}{ab}, \quad 14$$

where Φ is the porosity, L is the total length of the fracture median axes in the XY plane, a, b are the dimensions of one cell of the grid, *c* is the third dimension of the grid that in case of 2D modeling is set to 1 m in 2D, and λ is the coefficient of linear approximation. Note that the formulation of the dependence of D on the pH is valid for pH values between 6 and 10.5 and temperatures between 30 °C and 90 °C.

The fact that the kinetics of glass dissolution is controlled by the product $C_v \times S_{sp}$ implies that the law of the glass dissolution has to be set separately for each cell in the equivalent porous media system.

3 Verification

3.1 Fracture network of a synthetic model: preparation of input data for reactive transport modeling

Although the principal goal of this study was to perform the reactive transport modeling at the scale of the glass canister and verify the applicability of the techniques proposed with the aim to construct an equivalent fracture model, one synthetic discrete fracture network (Figure 4) was generated by the FRAGMA semi-stochastic generator [52].

When modeling the glass aqueous alteration applied to this discrete model, glass and water media were represented in two separate zones: the glass zone (depicted in purple in Figure 4b) and the fracture zone (depicted in green in Figure 4b).

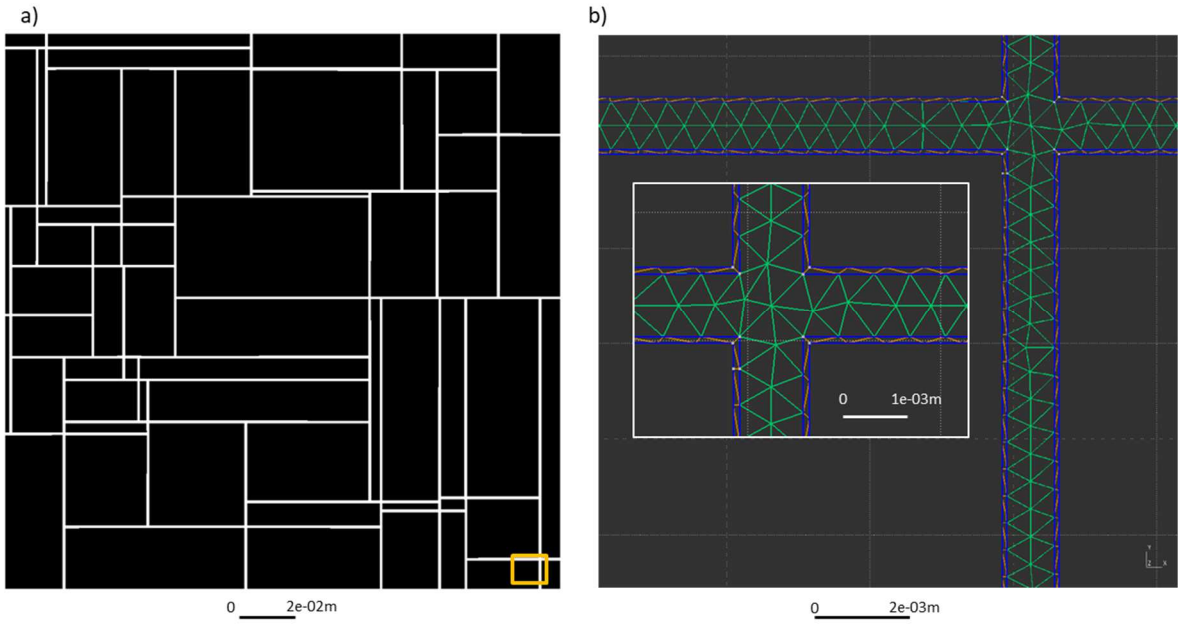

Figure 4 a) Image of the synthetic fracture network. Fractures have a constant aperture equal to 1 mm. The orange box shows the position of the mesh represented in b. Black pixels denote glass matrix, white pixels indicate fractures; b) fragment of the mesh used to run RTM. Cells in green belong to the water geochemical unit, while cells in blue belong to the glass geochemical unit. Total number of cells of the discrete fracture network is 24300. The thickness of the glass film is 0.1 mm. The total length of all walls of the fracture network is 5.93 m.

In accordance with the GRAAL formalism, both water in the fracture zone and glass in the glass zone were represented by liquid media. The glass zone was modeled by a one-mesh thickness layer at the interface with the fracture zone. The glass zone acted as a source of material and had a concentration given by (15):

$$C_v = \frac{\sum M_g}{\sum S * a/2}. \qquad 15$$

Using the geometrical properties of the fractures, equations (16) and (17) can be modified to yield the two parameters controlling the kinetics of glass dissolution. Depending on the modeled fracture network, these were determined as defined:

$$S_{sp} = \frac{\sum S}{\sum M_g}, \qquad 16$$

$$\text{half saturation} = \frac{\lambda D_{PRI} dm_{PRI}}{v_{hyrd}} \times \frac{2}{a} = \frac{\lambda dm_{PRI}}{v_{hyrd}} \times \frac{2}{a} \times D_o [OH^-]^n \exp\left(-\frac{E_a}{RT}\right), \qquad 17$$

where $a/2$ is the half-aperture of the fracture: only half of the aperture was used to account to the fact that each fracture wall «sees» only half of the solution present in the fracture.

The use of the discrete fracture modeling approach ruled out the necessity of the calculation of the equivalent hydraulic and diffusive parameters. However, it presented a big challenge due to its demand for the fine meshing, and as a consequence, high calculation time.

3.2 Results of the RTM applied to the synthetic case

As a first step, we conducted the RTM applied to the discrete fracture network model and its equivalent porous medium model of the synthetic fracture network to demonstrate the relevance of the techniques used to construct the equivalent continuum model.

The discrete fracture network system consisted primarily of the finely meshed glass fracture and secondly of two reservoirs of dimensions (0.064 m × 0.2 m), connected to both sides of the fracture network (Figure 5a). These two reservoirs were filled with water and interconnected *via* the glass fracture network.

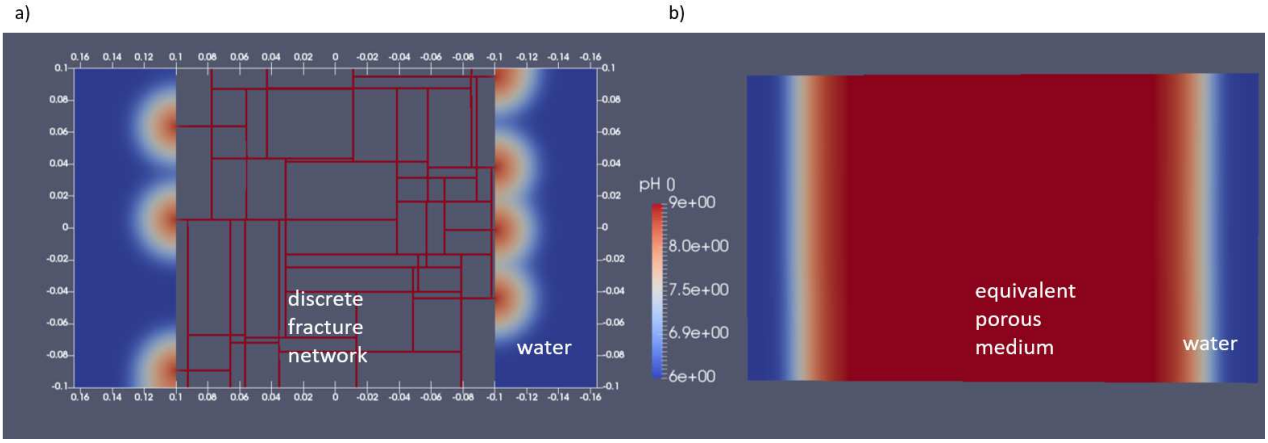

Figure 5 Physical representation of the system comprising two reservoirs and the synthetic facture network in the framework of a) the discrete model and b) the equivalent porous media model. X and Y axes are in m.

Table 3 summarizes the reactive transport input parameters of the discrete fracture network model. Hydraulic conductivity in water was estimated by fluid mechanics modeling from the iterative calculation, taking into account the velocity generated by the temperature differences between two opposite boundaries of the reservoirs separated by three ideal fractures of 1 mm aperture (Figure 15 in Appendix). The glass geochemical unit is represented by a liquid in which all glass is concentrated, and the porosity of this unit is equal to 1. This concentrated glass acts as a source of material readily available at the glass / water interface.

Table 3 Reactive transport parameters used to model the glass aqueous alteration in the synthetic fracture network described explicitly (discrete fracture network approach).

Geochemical unit	Porosity	Pore diffusion coefficient, m^2/s	Hydraulic conductivity coefficient at 25 °C, m/s	T,°C	C_v, g/l	S_{sp}, m^2/g	Half-saturation, molal
Glass	1	1×10^{-09}	-	90	3.49×10^{-04}	5.73×10^{-09}	3.07×10^{-11}
Water	1	1×10^{-09}	1	90	-	-	-

N.B. During the computation the hydraulic conductivity coefficient is recalculated in accordance to the temperature of the system by the reactive transport code HYTEC [9,10].

The equivalent porous medium model was composed of the grids of porosity, equivalent hydraulic conductivity (Figure 6 a–b), equivalent directional diffusion coefficient, and parameters requested to

specify the glass dissolution kinetic law, such as equivalent glass concentration, equivalent glass specific surface, and the half-saturation coefficient.

The values of the directional tortuosity were obtained by analyzing the regressions of the directional mean square displacements *vs.* time for each cell of the porous media. The examples of these regressions are illustrated in Figure 7. Subsequently, the tortuosity values were used to calculate the grids of diffusion coefficients shown in Figure 6 c–d.

Figure 8 depicts the results of particle concentration evaluation in the discrete fracture network and in its equivalent porous medium. From the curves of the concentration evolution, it is clear that the particles diffused in a similar manner in both media, and no significant differences were found. A discrepancy in concentration was regularly noticed only in cell (2,2). The results of particle tracking indicated that this cell was visited less frequently when the synthetic fracture network was replaced by its equivalent media. This slight divergence in the obtained concentrations was considered acceptable. Overall, the similarity of the concentration profiles was encouraging and indicated that the proposed approach based on the random walk could be applied for calculating the equivalent diffusion in the fractured zones of the glass block where the fracture density is significant, such as the peripheral parts of glass block fracture networks.

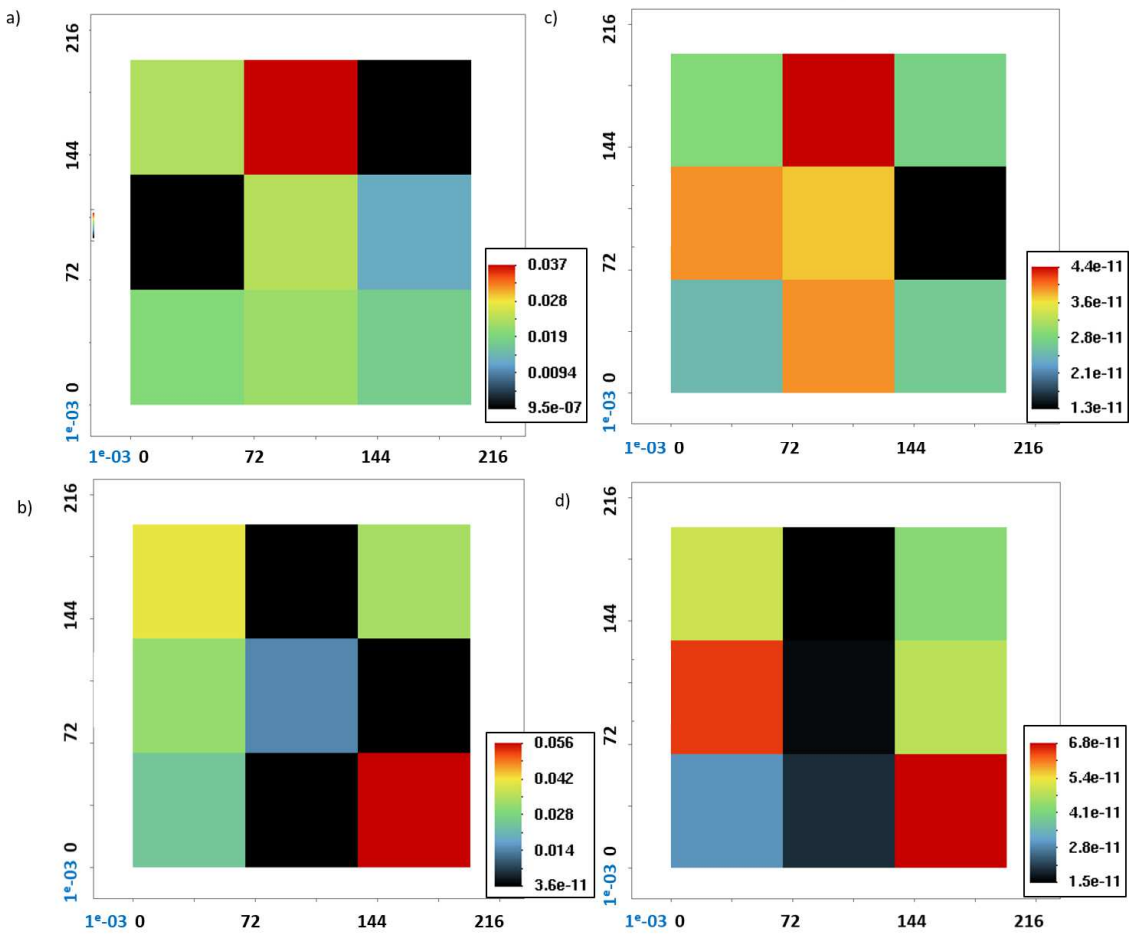

Figure 6 Results of the calculations of the equivalent parameters for the synthetic fracture network. Grids of: a, b) the equivalent directional hydraulic conductivity (m/s) in X and in Y; c, d) the equivalent directional diffusion coefficient (m^2/s) in X and in Y. Both axes are in m.

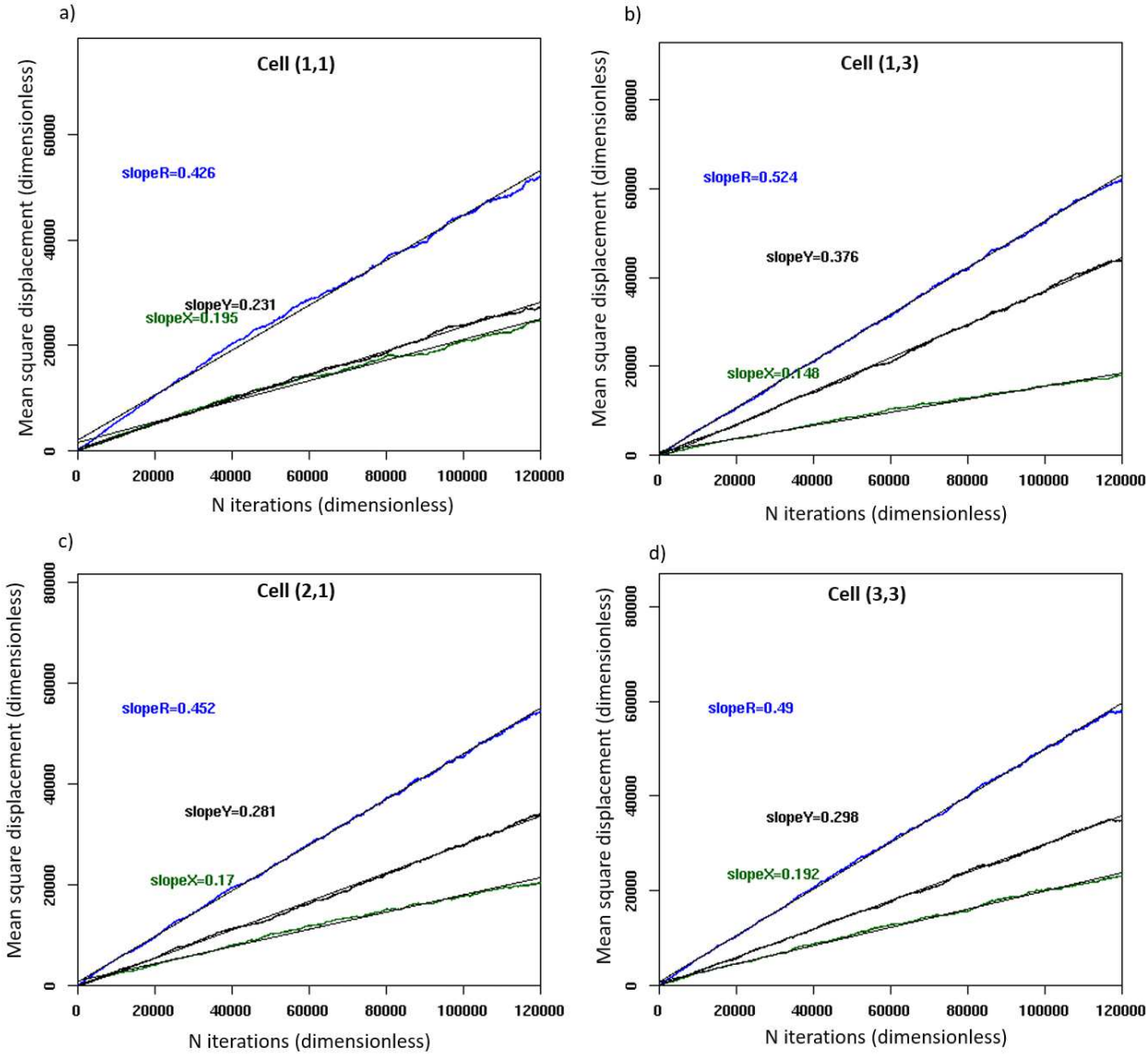

Figure 7 a–e) The mean square displacements ($\langle r^2 \rangle$ - in blue, $\langle x^2 \rangle$ – in green, $\langle y^2 \rangle$ –in black) vs. time of 2000 walkers for the synthetic fracture network. Plots are shown for the cells (1,1), (1,3), (2,1), (3,3) of the output grid presented in Figure 8d.

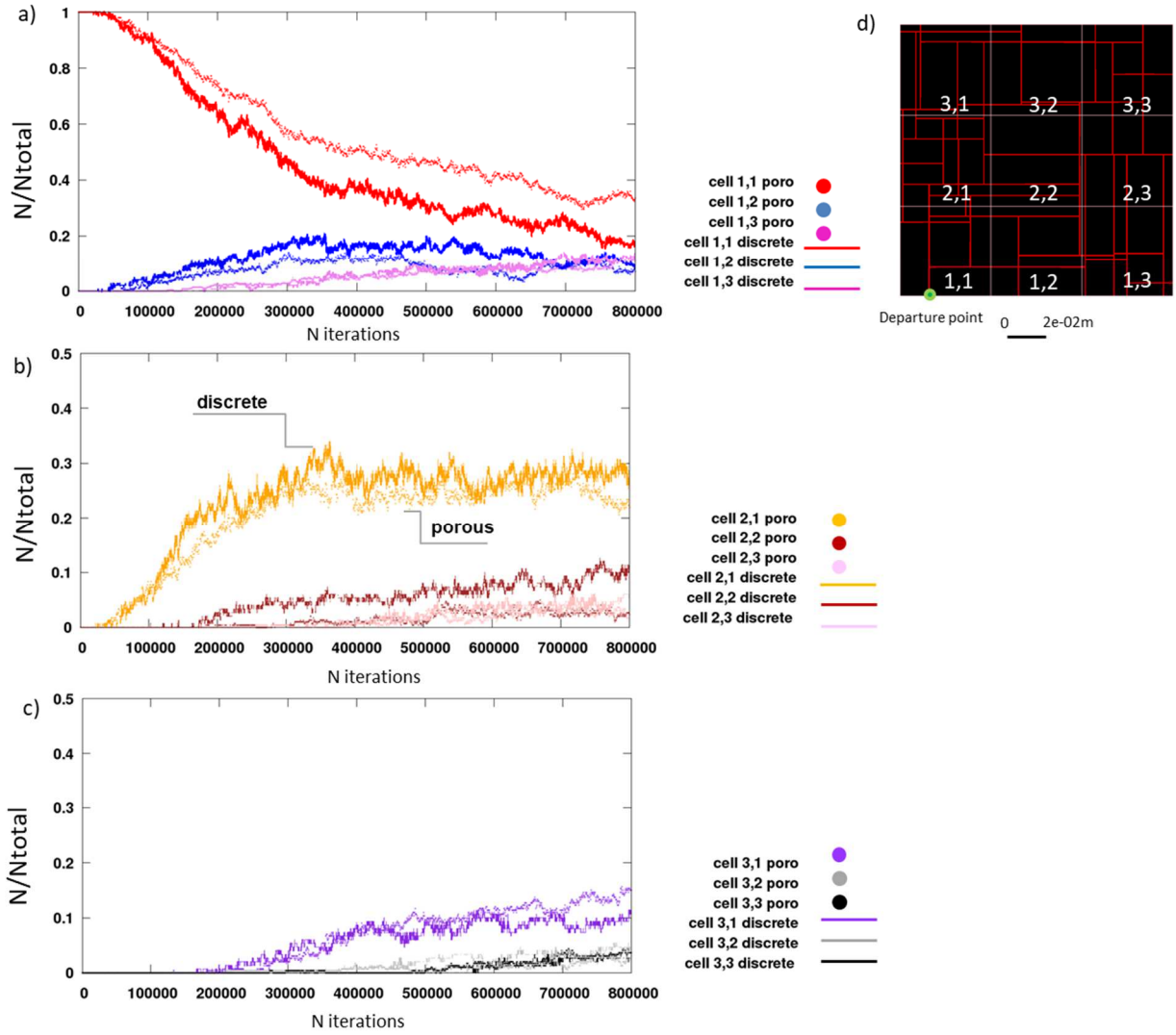

Figure 8 a–c) Evolution of particle concentration in the cells, obtained by tracking 500 independent particles undergoing Brownian motion in the discrete and the equivalent porous media. d) Scheme showing the synthetic discrete fracture network and the positions of the cells used in the legend of the graphics on the left.

Similarly to the discrete fracture network model, two water-bearing zones were added to the left and to the right of the equivalent porous media, such that the same water volume was available for both models in the glass alteration (Figure 5b). These supplementary meshes formed the water geochemical unit and were initialized with the same parameters, namely the diffusion coefficient and the hydraulic conductivity coefficient, as the water geochemical unit of the discrete model (Table 3).

The results of the RTM of ISG aqueous degradation obtained by the discrete and the equivalent continuum approaches are presented in Figure 9. The values of the alteration rate are correctly computed and their evolution can be easily explained in view of the kinetic regimes of the alteration of borosilicate glass reported in [53]. Specifically, after the initial dissolution rate regime ended around 8 h, a rate drop regime occurred until a residual rate was reached, which is four orders of magnitude lower. The differences of the absolute values of the alteration rate can be explained from the angle of the local chemical effects, *i.e.* saturation in silica was attained faster locally in the case of the discrete model, which leads to the creation of the passivating interface in the middle of cracks and slows down the alteration. In the case of the porous medium model, the alteration progressed

more homogeneously. This justification is supported by the results of the modeling. when the dependence of dissolution rate on pH and saturation was not taken into account. In fact, values of the glass alteration rate found by modeling the alteration at the constant dissolution rate by discrete and equivalent porous models were very close (Figure 16 in Appendix).

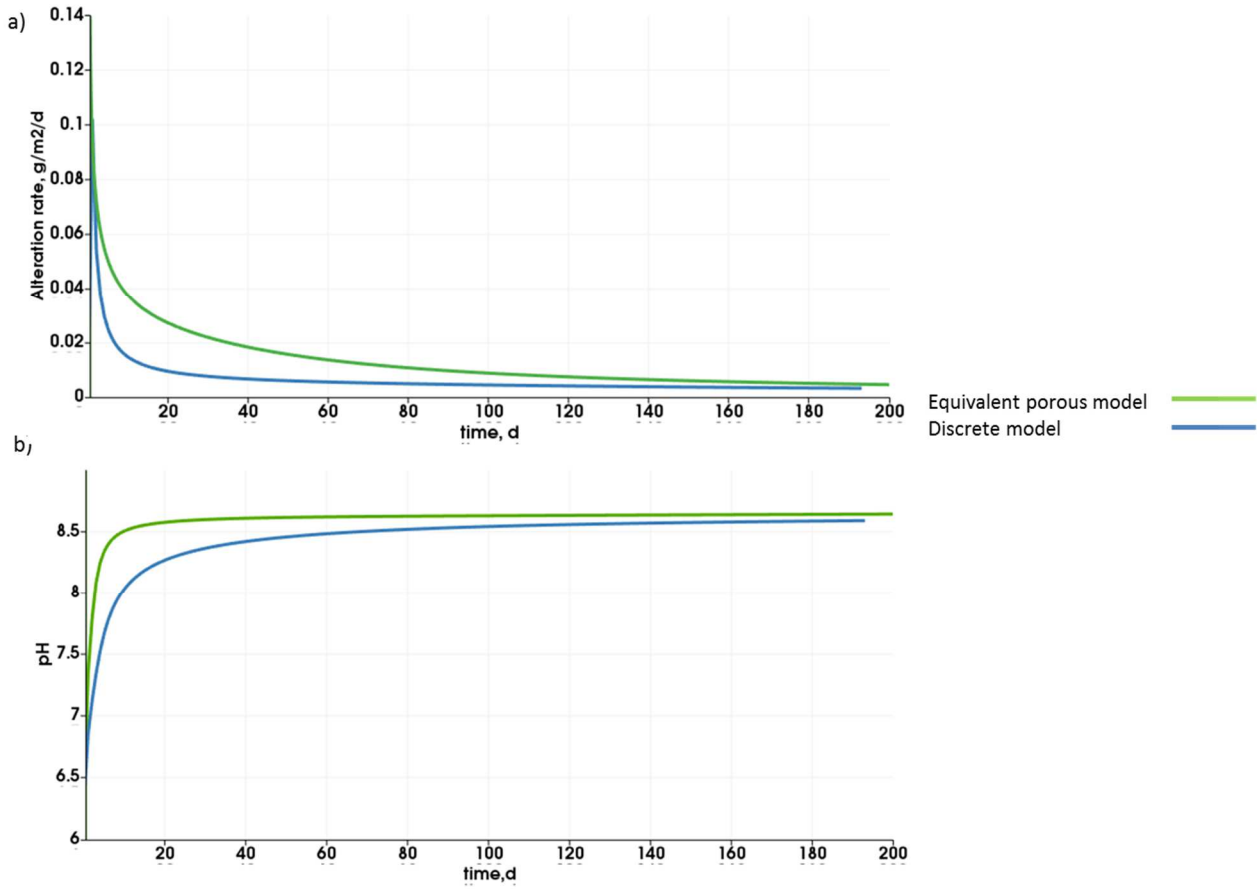

Figure 9 Results of the reactive transport modeling by the discrete fracture approach and by the equivalent continuum approach in the diffusive mode: a) the glass alteration rate obtained from boron concentration averaged over the water zones, b) evolution of the solution pH.

This application was performed to demonstrate the validity of the techniques proposed to compute the equivalent diffusive, hydraulic and alteration kinetics controlling parameters, obtained by comparing the results of the glass aqueous degradation found by the discrete fracture network model and the equivalent porous medium model. Given both the profiles of the alteration rate evolution and the pH evolution, it is evident that the equivalent porous medium model yielded results comparable with those of the discrete fracture network model. This is especially appealing in view of the fact that the rate of the calculation by the equivalent porous medium is much faster. This undoubtedly represents a significant advantage and implies that the model applicable at the industrial glass canister scale, or even under different scenarios of repository evolution. Table 4 presents the values of the time requested to execute simulations of the aqueous alteration applied to the synthetic discrete fracture network and to its equivalent porous media system. The RTM could not be run in convective mode applied to the discrete model of the synthetic case. However, this was realized for the equivalent porous model. The fluid movement in this simulation was generated by the temperature gradient imposed to the left (80 °C) and to the right (90 °C) walls of the water reservoirs (Figure 10).

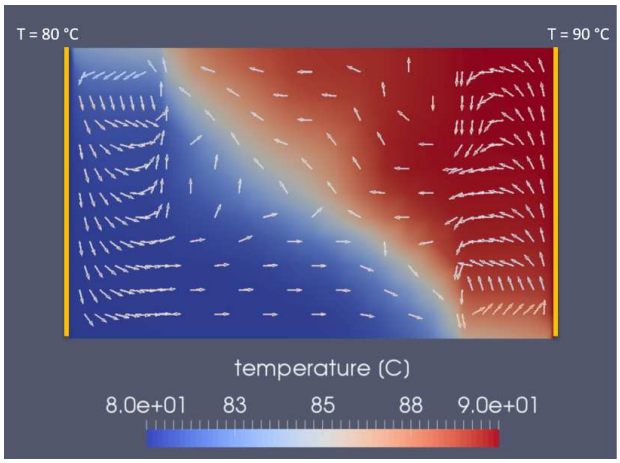

Figure 10 Equivalent porous media model: temperature field and directions of fluid movement.

The results of the glass aqueous alteration in convective mode can be found in Figure 17 in Appendix.

Table 4 Comparison of the time requested to conduct the RTM by the discrete fracture model and the equivalent continuum model. Number of processors was equal to 16 for all modeled cases.

Simulated time, year	Transport	Execution time, d	
		Discrete Fracture Model	Equivalent Continuum Model
1	Diffusion	87	0.22
1	Diffusion + Convection	-	15.1

4 Application

4.1 Application at the scale of the vitrified glass canister in diffusive and convective modes

Although this study focuses on the construction and the application of a 2D model of a nuclear glass fracture network at scale 1, its extension toward a simplified 3D model is feasible. Glass canisters, being perfect cylinders, have a natural axis of symmetry which has been used for the thermo-mechanical simulations at the glass canister scale [54]. Thus, the use of cylindrical coordinates was opted for in this study (Figure 11a).

The equivalent porous medium models of the training image fracture network and of three realizations of the fracture network equivalent tessellation were used. All models are composed of two geochemical units, the equivalent porous media unit and the water (reservoir) unit. The equivalent porous media unit is described by the map of porosity, equivalent hydraulic conductivity, equivalent directional diffusion coefficient, local direction of anisotropy[6] and parameters defining the glass dissolution kinetic law. Each grid was made up of 4 × 21 meshes, each mesh had dimensions of $5.168 \times 10^{-2} \times 4.964 \times 10^{-2}$ m. The water unit represented a hollow cylinder with a height equal to

[6] The rotation angle is defined as the angle associated with the largest axis of a fracture and the horizontal plane. The grid of the rotation angle is identical for all modeled cases and was employed to introduce the directional anisotropy of the hydraulic conductivity and the diffusion.

1.13244 m and internal and external radii equal to 0.2067 m and 0.2217 m, respectively. The total volume of the water zone was 35 L and reflected the amount of water initially present in contact with the glass canister in the ALISE experiment (Section 1.2). Figure 11 b–c shows the representation of the equivalent porous medium model at the glass canister scale, used to conduct RTM in diffusive and convective modes.

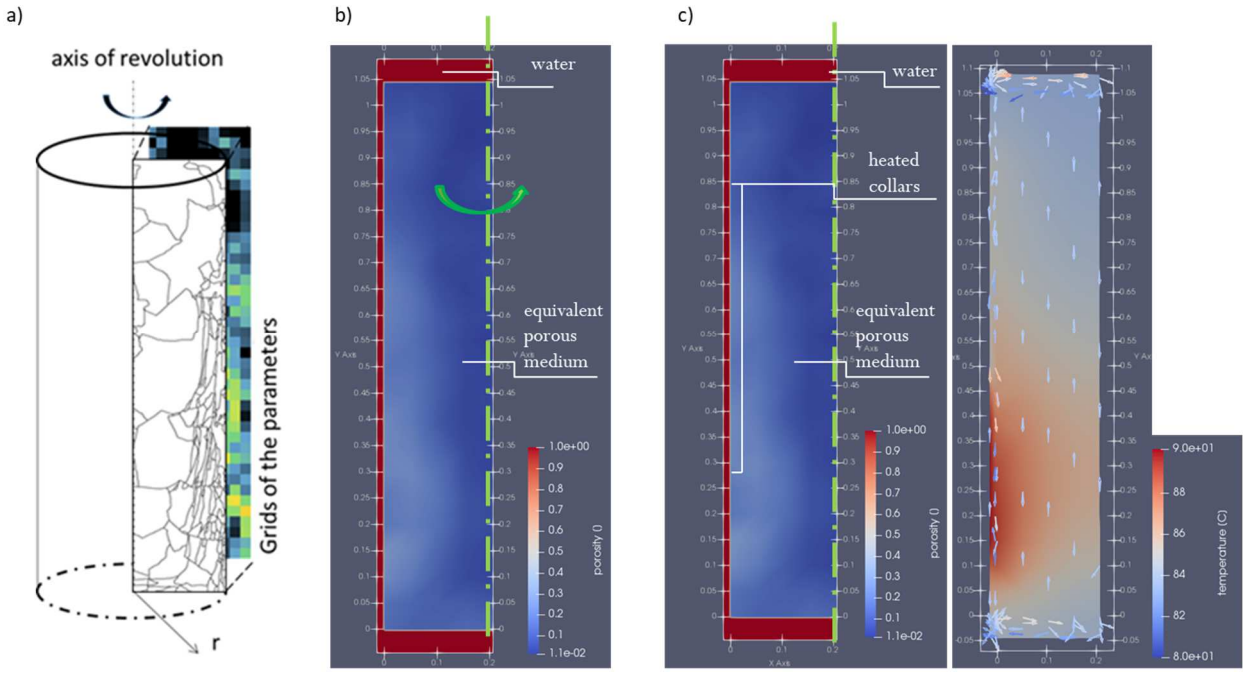

Figure 11 a) Conceptual representation of a simplified 3D model with cylindrical coordinates, b) representation of the equivalent porous medium model used to study the glass aqueous alteration in diffusive mode. The zero flux condition was imposed to the axis of revolution. c) Representation of the equivalent porous medium model used to study the glass aqueous alteration in convective mode. RTM was conducted with consideration of the following limiting conditions: upper heated collar – constant temperature at 80 °C, lower heated collar – constant temperature at 90 °C, axis of revolution – zero flux. X and Y axes are in m.

Results of RTM of the ISG glass aqueous alteration are given in Figure 12 for the diffusive mode and in Figure 13 for coupled diffusive and convective modes. Before proceeding to examine the results of these simulations, it is necessary to look at the interpretation of the experimental data.

4.2 Experimental results from ALISE unit

The results from the ALISE experiment are documented in [55,11].

Based on the detailed analysis of the concentration of the boron tracer element, the pH and the glass alteration rate, the study in [11] reported five phases of alteration. Phase 1, from 1 to 30 days: the initial phase characterized by a rapid transition from the initial rate regime to the rate drop regime reflected by the sharp increase of the released altered glass per unit time and the quick increase of the pH. Phase 2, from 30 to 550 days: gradual decline of the alteration intensity characterized by progressive decrease of the alteration rate (from ~0.3 g/d to ~0.2 g/d) and the slow increase of the pH (from ~8.9 to ~9). Phase 3, from 550 to 1400 days: interchange between the regime of the alteration rate recovery [56] and the regime of the alteration rate drop. Phase 4, from 1400 to 1700 days: recovery of the alteration rate, with an increase of the alteration rate (from ~0.15 to ~0.21) and the significant increase of the pH (from ~9.15 to ~9.25). The final phase (1700 to

2700 days) involved external interventions, which disturbed the experiment and thus did not allow for a proper interpretation.

4.3 Diffusive mode simulation

The modeling results of the average total dissolved boron concentration in water, the average pH in water, and the glass alteration rate are shown in Figure 12.

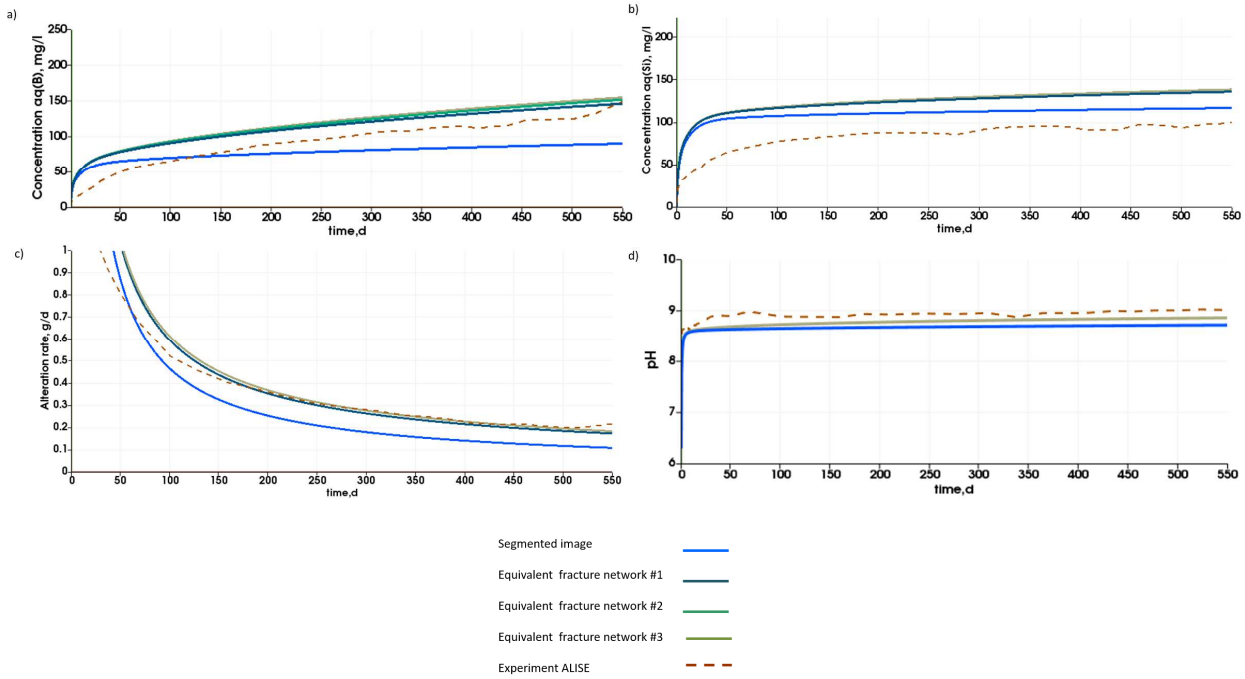

Figure 12 Results of the RTM of the aqueous alteration in the diffusive mode at the scale of the nuclear glass canister: a) average concentration of all aqueous species containing boron present in the solution, b) average concentration of all aqueous species containing silicon present in the solution, c) overall glass alteration rate obtained by total boron release, d) evolution of the solution pH. Experimental results of the ALISE test are documented in [11]. It should be noted that the experimental results and the modelling results could be compared only for the first 550 days (presented on the figure), because later the ALISE experiment displays phases of (i) the alteration resumption that is not considered in the applied version of the geochemical model and (ii) the impact of the chemical perturbations due to external interventions.

A comparison of these results with experimental data reveals that the first part of the alteration (0–550 d) was correctly reproduced. The simulations in diffusive mode exhibit the same pattern of the alteration regimes transition as the ALISE experiment: a sharp decrease from the initial alteration rate in the first tens of days followed by a period of the gradual alteration rate decline and the stabilization of pH. Moreover, for this first period, the average total dissolved boron and silicon concentrations for three equivalent fracture networks are close to the experimentally measured concentrations. However, the results of the RTM applied to the segmented image are less compatible: this less intensive glass alteration is believed to be related to an underestimation of glass fracture surface available for the alteration. Indeed, according to Table 1, internal fracture surface of the segmented image is 2.5 times lower than that of the equivalent tessellations. Unfortunately, the fracture network surface of the ALISE bloc was not determined, such that no comparison with the model is possible.

The simulation of the second part of the alteration (550–2700 d, Figure 18 in Appendix) was not attempted. Indeed, the ALISE experiment displays phases of the alteration resumption from the 550th

day, during which the glass is again significantly altered. The GRAAL model (in the version that was used) does not take this phenomenon into account, since it is not expected in repository environments. The perturbations of the chemical environment due to maintenance of the apparatus in phase 5 of the experiment are not relevant either.

In summary, the proximity of the results of the RTM applied to the equivalent tessellations with the experimental results enables us to argue that (i) the chosen fracture network equivalent tessellations are representative of the ALISE glass block fracture network, and (ii) the technique proposed to construct glass block equivalent porous model are relevant and could be relied upon.

The comparison of several principal parameters (pH, boron concentration, silicon concentration, rate of the glass alteration) obtained from the experiment and the modeling shows clearly their proximity. The data set is not sufficient to completely qualify the model, however the fact that integrative data (pH and Si notably, clear indicators of the chemical reactions and the transport driver) gives confidence in the proposed model. It means that the chosen fracture network equivalent tessellations are representative of the ALISE glass block fracture network (because they are leached in the same manner). Therefore, the technique proposed to construct glass block equivalent porous model are proved to be relevant and could be relied upon.

4.4 Thermo-convective mode simulation

Due to experimental constraints, the ALISE experiment did not display temperature gradients and therefore not thermo-convection. However, heat release by the wastes and diffusion in the host rock are bound to create temperature gradients in repository applications, including at the waste scale. Simulations with thermo-convection were therefore conducted to evaluate the impact of the water convection on the alteration in the fractured nuclear glass blocks. They gave similar overall results (Figure 13), with a fast initial alteration rate and the following rate drop regime to the residual rate. During this time the alteration rate dropped from ~70 g/d (after 12 h) to ~0.065 g/d, and the pH increased from ~8.45 to ~8.94. Figure 14 shows that the initial rate was much higher in the presence of thermo-convection. In fact, once the convection was installed, it stimulated the renewal of water inside the glass fracture equivalent media with fresh water from the outer reservoir. This resulted in the immediate increase of the dissolution rate. Then, when the saturation in silica became high, the reaction affinity diminished and the rate started to drop. The transition from the initial rate regime to the residual rate regime was shorter for the diffusive case in comparison to the convective case. Although the average total concentration of silica in water was lower in case of pure diffusive transport, the effect of local arrivals on silica saturation was more important.

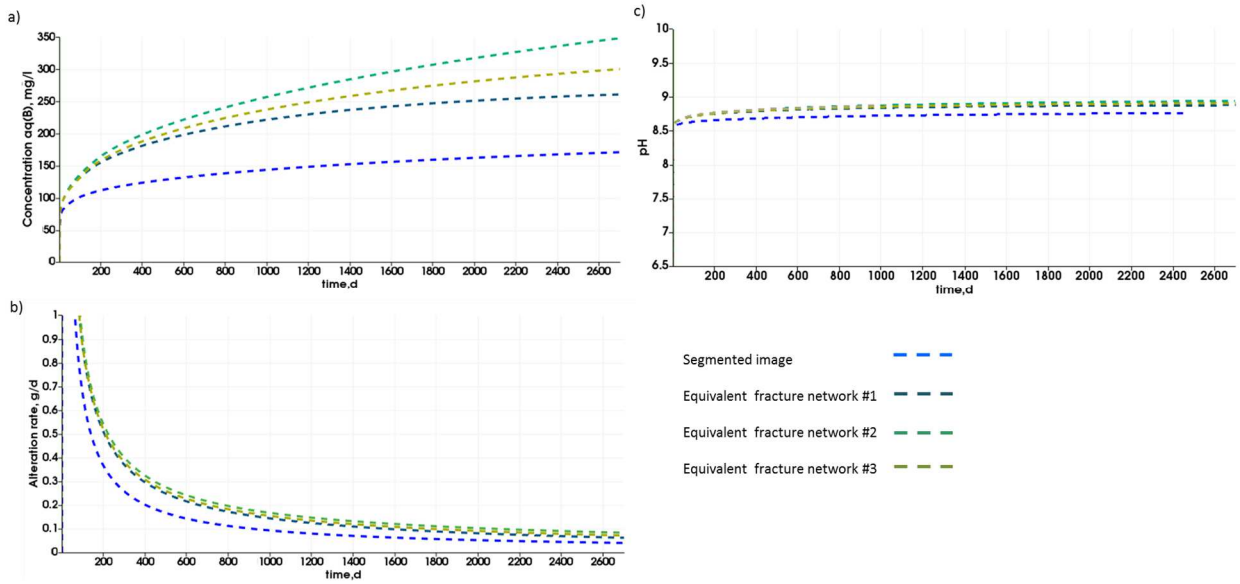

Figure 13 Results of the RTM of the aqueous alteration at the scale of the nuclear glass canister: a) average concentration of all aqueous species containing boron present in the solution, b) evolution of the solution pH, and c) overall glass alteration rate obtained from total boron release. Both diffusion and thermo-convection caused by the imposed temperature difference were considered.

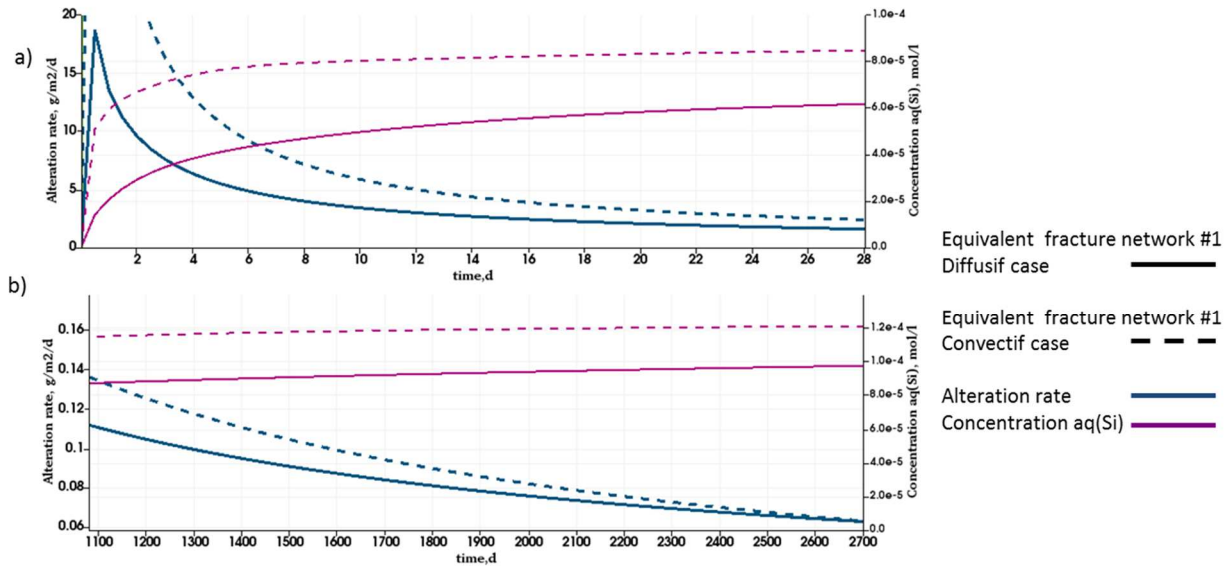

Figure 14 Evolution of the average total concentration of silica present in water and the alteration rate: a) in the short-term and b) in the long-term.

5 Discussion

Regarding the project feasibility study, it is important to consider several scenarios in the geological repository evolution. That is why it is essential to compare the results of the borosilicate glass alteration obtained in diffusive and convective modes. In this study, we do not aim at reproducing a scenario of repository conditions, where the fluid movement would potentially result from the heat release due to radioactivity. Nevertheless, the results of the modeling presented in this paper

provide a preliminary idea about the impact of water flow on the intensity of the glass alteration at the scale of one canister.

According to the results presented in Figures 12–14, glass degradation was favored by water convection. Twelve hours from the start of the alteration, the glass alteration rate was four times higher compared to the no-flow case. The effect was, however, less significant once the solution became saturated in alteration products. Indeed, for the fracture tessellation #1, as an example, the glass altered rate in the convective flow conditions at the 20^{th} day of alteration made up only 4.8% of the initial rate and was 1.54 times higher than the alteration rate in the pure diffusive movement conditions. However, it is important to mention that the gradient imposed in the presented case was significant (10 °C) and does not reflect the situation in repository conditions.

In future studies, it would be interesting to conduct reactive transport modeling in conditions that are more representative of the repository. Heat sources could be specified according to specific scenarios: time of water intrusion, spacing between canisters, and heat exchange with the host rock. The methodology developed in this paper could then be extended to 3D simulations. Application to industrial purposes would require further research to understand and quantify the phenomena that would govern (i) the alteration of the borosilicate glass in presence of all the components of the nearby field (*e.g.* iron of the overpack, clay of the COx), (ii) the transport of the alteration products with the COx water in the conditions of the argillite pores clogging, and (iii) the mechanisms of glass alteration and solutes migration in presence of hydrogen originated from radiolysis and corrosion of the overpacks.

According to multiple studies [57-61], in presence of iron, glass alteration is fostered by the precipitation of iron silicate species. The formation of these secondary phases modifies the chemical equilibrium in the aqueous solution, acting as a “silicon pump” and, as a consequence, increases glass alteration. Regarding the interactions with the COx water, studies [62-64] show that the pH of the water of the repository site and the availability of magnesium in solution can affect the transient regime, where dissolution rate drops rapidly and the residual rate. In fact, magnesium secondary phases could maintain glass alteration by consuming silicon. Nevertheless, in absence of a renewal of magnesium or in the case of decrease of the pH, the expected residual rate was reported close to that measured in pure water [65,62].

In accordance with the current vision of the high-level vitrified waste alteration model presented by ANDRA [65], the first phase of glass alteration would take place in unsaturated conditions resulting from partial re-saturation of the vicinity of the cell and the counter-effect of hydrogen release due to radiolysis and anoxic corrosion of metallic components, which could last from several thousand to tens of thousands of years. In consideration of the possibility of a high relative humidity in the storage conditions, studies aiming at the understanding of the mechanisms of glass alteration in the vapor phase have been initiated. From the experimental results conducted so far, it can be understood that the reactions occurring between glass and water are the same for alteration in aqueous medium and unsaturated water vapor. However, the rate controlling reaction mechanism and the driving force for alteration are different in both cases [66]. The difference arises largely from the changes in water chemistry, as a result of the extremely small volume of water available for reaction in the unsaturated case. The various results from vapor hydration experiments suggest that the alteration in vapor phase is not simply an extreme case of glass alteration in aqueous medium at

a very high S/V [67]. The precipitation of secondary phases seems to be the strongest driving force for alteration in vapor phase at high temperature and low solution volume.

Moreover, presently there is no clear vision on the possibility of the gas to coexist with the water. In fact, it is necessary to understand in further detail how the repository re-saturation will happen. Although, according to ANDRA [68], hydrogen presence will not imply significant overpressure in water, it is still uncertain how the re-saturation will occur precisely in different compartments of the repository, what will be the relative permeability of the hosting rock and the infilling materials of the repository, and how the transport of the solutes in the biphasic condition will differ from that in the saturated condition.

In general, our model can be evolved to take into account the above-cited phenomena. Certainly, in case of the presence of both gas and water phases inside the fracture network of vitrified canisters, it will be mandatory to change the techniques of the permeability and effective diffusion calculation [69,70], and take into the account saturation of both wetting (water) and non-wetting (gas) phases, as well as the capillary pressure [71]. Moreover, in the future, the geochemical part of the model should be enhanced, such that the interactions of the elements of the nearby field could be accounted for. This will require an upgrade of the geochemical model and could also require accounting for the change of fracture aperture, since the hypothesis of isovolumetricity would not be valid anymore. Moreover, the temporal porosity change related to the swelling of argillites minerals [72,73] would be probably worth considering when estimating the temporal evolution of the hydraulic/diffusive properties of glass canister fracture network.

Another possible evolution of the upscaling is towards a hybrid model. Indeed, the glass canister fracture network exhibits strong non-stationarity: large sparse fractures in the center, opposed to fine, dense fractures close to the periphery. A hybrid model could be devised, with explicit fractures at the core of the canister and equivalent medium on the finely fractured peripheral area. This change of the modeling approach should be considered with regard to the calculation capabilities of the applied reactive transport code. This is because, at the present time, it is hardly possible to run this type of model at the scale of the glass canister, especially when the convection, originated by temperature gradient, is taken into account.

6 Conclusions

Coupled chemistry-transport models must be used to quantitatively assess the corrosion of the vitrified fractured glass containing long-lived high-level nuclear waste. Having been restricted to laboratory examinations for a long time, the present study gives an example of how such models can be used for geometries (2D and simplified 3D) and time scales relevant for performance assessment. Given the difficulty of performing reactive transport modeling applied directly to the discrete representation of the glass fracture network at the scale of glass canister, we focused here on the construction of its equivalent porous model. Special attention was paid to the calculation of the reactive transport parameters such as porosity, tortuosity, diffusion coefficient, hydraulic conductivity, and glass alteration kinetic parameters. First, the validation of the applicability of the proposed techniques was accomplished by conducting reactive transport modeling applied to a synthetic two-dimensional fracture network in the scope of the discrete model and the equivalent porous model. Second, the equivalent porous model was applied to four representations of the glass

fracture network. The reactive transport modeling was performed in cylindrical coordinates in diffusive and convective modes. The results of the quantity of altered glass were then compared with experimental results obtained of the long-term aqueous alteration test of a non-radioactive full-scale nuclear glass block. Reasons were provided to explain the minor differences. Although the reproduction of one particular scenario in the conditions of the repository was not the objective of this study, the presented results gave a preliminary indication of the impact of thermo-convection on the glass alteration at the scale of one canister and demonstrated the feasibility of the glass corrosion reactive transport modeling under different scenarios of repository evolution.

The presented model focused on glass-water interaction in conditions that do not correspond to the repository conditions. Nevertheless, the model could be extended or re-adapted such that different scenarios of canister evolution might be considered. The strength of this work, started in [8], is within the proposal of a complex workflow and data integration process that allows the estimation of the impact of fracturing on the glass corrosion, by taking account fracture network variability and different limiting conditions.

Acknowledgements

The authors wish to thank P. Frugier (CEA Marcoule) and T. Le Borgne (Rennes-1 University) for fruitful discussions. We thank the two anonymous reviewers for their constructive critics, suggestions and comments.

Research data availability

The raw/processed data required to reproduce these findings cannot be shared at this time, as the data also forms part of an ongoing study. The data that support the findings of this study will be available at a later date from the corresponding author, Frederic Bouyer, upon request.

References

1. ANDRA: Rapport Andra CG-TE-D-NTE-AMOA-SR1-0000-15-0060 – « Dossier d'options de sûreté - Partie exploitation ». In. (2016)
2. ANDRA: Dossier 2005 Argile - Tome Évolution Phénoménologique du Stockage Géologique. In: ANDRA (ed.). pp. 1-523. (2005)
3. Zhang, C.-L.: Thermo-hydro-mechanical behavior of clay rock for deep geological disposal of high-level radioactive waste. Journal of Rock Mechanics and Geotechnical Engineering (2018). doi:https://doi.org/10.1016/j.jrmge.2018.03.006
4. Cvetkovic, V., Painter, S., Outters, N., Selroos, J.O.: Stochastic simulation of radionuclide migration in discretely fractured rock near the Aspo Hard Rock Laboratory. Water resources research **40**(2), W02404 (2004). doi:10.1029/2003wr002655
5. Nykyri, M., Nordman, H., Loefman, J., Poteri, A., Marcos, N., Hautojorvi, A.: Radionuclide release and transport RNT-2008. In., vol. POSIVA--08-06, p. 164. Finland, (2008)
6. Pierce, E.M., Frugier, P., Criscenti, L., J., Kwon, K.D., Kerisit, S.N.: Modeling Interfacial Glass-Water Reactions: Recent Advances and Current Limitations. International Journal of Applied Glass Science **5**(4), 421-435 (2014). doi:10.1111/ijag.12077
7. Gin, S., Abdelouas, A., Criscenti, L.J., Ebert, W.L., Ferrand, K., Geisler, T., Harrison, M.T., Inagaki, Y., Mitsui, S., Mueller, K.T., Marra, J.C., Pantano, C.G., Pierce, E.M., Ryan, J.V., Schofield, J.M.,

Steefel, C.I., Vienna, J.D.: An international initiative on long-term behavior of high-level nuclear waste glass. Materials Today **16**(6), 243-248 (2013).
8. Repina, M., Renard, D., Bouyer, F., Lagneau, V.: Coupling image analysis and thermo-mechanical simulation results to produce a model of the fracture network in a nuclear glass canister. Journal of Nuclear Materials **522** (2019). doi:10.1016/j.jnucmat.2019.05.013
9. Van der Lee, J., De Windt, L., Lagneau, V., Goblet, P.: Module-oriented modeling of reactive transport with HYTEC. Computers & Geosciences **29**(3), 265-275 (2003).
10. Lagneau, V., van der Lee, J.: Operator-splitting-based reactive transport models in strong feedback of porosity change: The contribution of analytical solutions for accuracy validation and estimator improvement, vol. 112. (2010)
11. Minet, Y., Chouchan, J., Mestre, J.: Altération du bloc SON68 01FID07/2 dans Alise à 106°C: résultats de l'essai longue durée (7,5 ans) et observations post mortem. In: CEA (ed.). pp. 1-67. (2013)
12. Frugier, P., Gin, S., Minet, Y., Chave, T., Bonin, B., Godon, N.,Lartigue, J.E., Jollivet, P., Ayral, A., De Windt, L., Santarini, G.: SON68 Nuclear glass dissolution kinetics: Current state of knowledge and basis of the new GRAAL model. Journal of Nuclear Materials **380**(1-3), 8-21 (2008).
13. Frugier, P., Minet, Y., Rajmohan, N., Godon, N., Gin, S.: Modeling glass corrosion with GRAAL. npj Materials Degradation **2**(1), 35 (2018). doi:10.1038/s41529-018-0056-z
14. Frugier, P., Chave, T., Gin, S., Lartigue, J.E.: Application of the GRAAL Model to Leaching Experiments with SON68 Nuclear Glass in Initially Pure Water. Journal of Nuclear Materials **392**(3), 552-567 (2009).
15. Minet, Y., Bonin, B., Gin, S., Frugier, P.: Analytic implementation of the GRAAL model: Application to a R7T7-type glass package in a geological disposal environment. Journal of Nuclear Materials **404**(3), 178-202 (2010).
16. Ferrand, K., Abdelouas, A., Grambow, B.: Water diffusion in the simulated French nuclear waste glass SON 68 contacting silica rich solutions: Experimental and modeling. Journal of Nuclear Materials **355**(1-3), 54-67 (2006).
17. Geisler, T., Janssen, A., Scheiter, D., Stephan, T., Berndt, J., Putnis, A.: Aqueous corrosion of borosilicate glass under acidic conditions: A new corrosion mechanism. Journal of Non-Crystalline Solids **356**(28-30), 1458-1465 (2010).
18. Donzel, N., Gin, S., Augereau, F., Ramonda, M.: Study of gel development during SON68 glass alteration using atomic force microscopy. Comparison with two simplified glasses. Journal of Nuclear Materials **317**(1), 83-92 (2003).
19. Verney-Carron, A., Gin, S., Frugier, P., Libourel, G.: Long-term modeling of alteration-transport coupling: application to a fractured Roman glass. Geochimica and Cosmochimica Acta **74**(8), 2291-2315 (2010).
20. Lagneau, V.: Simulation of coupled geochemical reactions and hydynamical processes in porous media -- application to CO2 storage and Uranium exploitation. Université Pierre et Marie Curie - Paris VI (2013)
21. Geuzaine, C., Remacle, J.F.: Gmsh: A 3-D finite element mesh generator with built-in pre- and post-processing facilities. International Journal for Numerical Methods in Engineering **79**(11), 1309-1331 (2009).
22. van der Lee, J.: Thermodynamic and mathematical concepts of CHESS. In: Paris, E.d.M.d., Fontainebleau (eds.). (1998)
23. Wolery, T.J.: EQ3/6, a software package for geochemical modeling of aqueous systems: Package overview and installation guide (Version 70). In., vol. UCRL-MA--110662-Pt1, p. 70. United States, (1992)
24. de Marsily, G.: Quantitative Hadrogeology: Groundwater Hydrology for Engineers. (1986).
25. Renard, P.: Modélisation des écoulements en milieux poreux hétérogènes. Paris Mines (1997)
26. Deng, H.: Upscaling Reactive Transport Parameters for Porous and Fractured Porous Media. Dissertation(Florida State University) (2009).

27. Durlofsky, L.J.: Numerical calculation of equivalent grid block permeability tensors for heterogeneous porous media. Water Resources Research **27**(5), 699-708 (1991). doi:doi:10.1029/91WR00107
28. Begg, S., R. Carter, R., Dranfield, P.: Assigning effective values to simulator grid-block parameters. (1989)
29. Christie, M.A.: Upscaling for Reservoir Simulation. SPE-37324-JPT **48**(11), 1004-1010 (1996). doi:10.2118/37324-JPT
30. Neuman, S.P.: Universal scaling of hydraulic conductivities and dispersivities in geologic media. Water Resources Research **26**(8), 1749-1758 (1990). doi:10.1029/WR026i008p01749
31. Zhou, Q.L., Hui Hai; Molz, Fred J. et al.: Field-Scale Effective Matrix Diffusion Coefficient for Fractured Rock: Results From Literature Survey. (2008).
32. Cushman, J.H., Bennethum, L.S., Hu, B.X.: A primer on upscaling tools for porous media. Advances in Water Resources **25**(8), 1043-1067 (2002). doi:https://doi.org/10.1016/S0309-1708(02)00047-7
33. Fernàndez-Garcia, D., Illangasekare, T.H., Rajaram, H.: Differences in the scale dependence of dispersivity and retardation factors estimated from forced-gradient and uniform flow tracer tests in three-dimensional physically and chemically heterogeneous porous media. Water Resources Research **41**(3) (2005). doi:10.1029/2004WR003125
34. Nos, J., Lagneau, V., Langlais, V.: Reactive transport upscaling at the Darcy scale: A new flow rate based approach raises the unsolved issue of porosity upscaling, vol. 34. (2011)
35. Whitaker, S.: Diffusion and dispersion in porous media. AIChE Journal **13**(3), 420-427 (1967). doi:10.1002/aic.690130308
36. Hornung, U. (ed.) Homogenization and porous media. Springer-Verlag, (1997)
37. King, P.R.: Transp Porous Med. Kluwer Academic Publishers (1989).
38. Noetinger, B.: The effective permeability of a heterogeneous porous media. Transp. Porous Media, 99-127 (1994).
39. Wood, B.D., Cherblanc, F., Quintard, M., Whitaker, S.: Volume averaging for determining the effective dispersion tensor: Closure using periodic unit cells and comparison with ensemble averaging. Water Resources Research **39**(8) (2003). doi:10.1029/2002WR001723
40. Nœtinger, B., Estebenet, T.: Up-Scaling of Double Porosity Fractured Media Using Continuous-Time Random Walks Methods. Transport in Porous Media **39**(3), 315-337 (2000). doi:10.1023/A:1006639025910
41. Renard P., d.M.G.: Calculating equivalent permeability: a review. Advances in Water Resources **20**(5-6), 253-278 (1997).
42. Renard, P., de Marsily, G.: Calculating equivalent permeability: a review. Advances in Water Resources **20**(5), 253-278 (1997). doi:https://doi.org/10.1016/S0309-1708(96)00050-4
43. Renard, P., Le Loc'h, G., Ledoux, E., Marsily, G., Mackay, R.: A fast algorithm for the estimation of the equivalent hydraulic conductivity of heterogeneous media. Water Resources Research **36**(12), 3567-3580 (2000). doi:10.1029/2000WR900203
44. Ougier-Simonin, A.: Propriétés mécaniques et de transport des verres fissurés. Université Denis Diderot - Paris 7 (2010)
45. Noetinger, B., Roubinet, D., Russian, A. et al.: Random Walk Methods for Modeling Hydrodynamic Transport in Porous and Fractured Media from Pore to Reservoir Scale. Transp Porous Med (2016).
46. Einstein. A., F.r.R.: Investigations on the theory of Brownian movement. (New York, N.Y. : Dover Publications) (1956).
47. Promentilla, M.A.B., Sugiyama, T., Hitomi, T., Takeda, N.: Quantification of tortuosity in hardened cement pastes using synchrotron-based X-ray computed microtomography. Cement and Concrete Research **39**(6), 548-557 (2009). doi:https://doi.org/10.1016/j.cemconres.2009.03.005
48. Nakashima, Y., Nakano, T., Nakamura, K., Uesugi, K., Tsuchiyama, A., Ikeda, S.: Three-dimensional diffusion of non-sorbing species in porous sandstone: computer simulation based on X-ray

microtomography using synchrotron radiation. Journal of Contaminant Hydrology **74**(1), 253-264 (2004). doi:https://doi.org/10.1016/j.jconhyd.2004.03.002
49. Sen, P.: Time-dependent diffusion coefficient as a probe of geometry. Concepts in Magnetic Resonance Part A **23A**(1), 1-21 (2004). doi:10.1002/cmr.a.20017
50. Gouze, P., Luquot, L.: X-ray microtomography characterization of porosity, permeability and reactive surface changes during dissolution. Journal of Contaminant Hydrology **120-121**, 45-55 (2011). doi:https://doi.org/10.1016/j.jconhyd.2010.07.004
51. Mitra, P.P., Sen, P.N., Schwartz, L.M.: Short-time behavior of the diffusion coefficient as a geometrical probe of porous media. Physical Review B **47**(14), 8565-8574 (1993). doi:10.1103/PhysRevB.47.8565
52. Crevoisier, D., Bouyer, F., Gin, S.: Semi-stochastic generator (FRAGMA) of 2D fractured media by mechanistic analogy. Application to reactive transport in a fractured package of vitrified nuclear waste. Computational Materials Science **50**(4), 1387-1398 (2011).
53. Gin, S., Beaudoux, X., Angeli, F., Jegou, C., Godon, N.: Effect of composition on the short-term and long-term dissolution rates of ten glasses of increasing complexity from 3 to 30 oxides. Journal of Non-Crystalline Solids **358**(18-19), 2559-2570 (2012).
54. Barth, N.: Sur la modélisation et la simulation du comportement mécanique endommageable de verres borosilicatés sous sollicitation thermique. Université de Strasbourg (2013)
55. Godon, N., Peuget, S., Bouyer, F., Angeli, F., Depierre, S., Pinet, O., Tribet, M., Boizot, B., Delaye, J.M., Dussossoy, J.L., Ollier, N., Gin, S., Jégou, C., I., R.: Référentiel scientifique sur le comportement à long terme des déchets vitrifiés : résultats de la R&D menée en collaboration avec les producteurs de déchets. In: CEA (ed.). pp. 1-425. (2012)
56. Fournier, M., Gin, S., Frugier, P.: Resumption of nuclear glass alteration: State of the art. Journal of Nuclear Materials **448**(1-3), 348-363 (2014).
57. Carrière, C.: Influence de la corrosion du fer sur les processus d'altération du verre : approche analytique multi-échelle., Université Pierre et Marie Curie - Paris VI (2017)
58. Neill, L., Gin, S., Ducasse, T., De Echave, T., Fournier, M., Jollivet, P., Gourgiotis, A., Wall, N.A.: Various effects of magnetite on international simple glass (ISG) dissolution: implications for the long-term durability of nuclear glasses. npj Materials Degradation **1**(1), 1 (2017). doi:10.1038/s41529-017-0001-6
59. de Combarieu, G.: Altération du verre de confinement de déchets type R7T7 en condition de stockage géologique., Université Paris XI - UFR Scientifique d'Orsay (2007)
60. Rébiscoul, D., Burger, Emilien, Bruguier, Florence, Godon, Nicole, Chouchan, Jean-Louis, Mestre, Jean-Pierre, Frugier, Pierre, Lartigue, Jean-Eric, Gin, Stephane: Glass-Iron-Clay interactions in a radioactive waste geological disposal: a multiscale approach. MRS Proceedings **1518**, 185-190 (2013). doi:10.1557/opl.2013.67
61. Arena, H.: Effets cumulatifs et compétitifs des éléments chimiques sur l'altération des verres nucléaires. (2016)
62. Jollivet, P., Frugier, P., Parisot, G., Mestre, J.-P., Brackx, E., Gin, S., schumacher, S.: Effect of clayey groundwater on the dissolution rate of the simulated nuclear waste glass SON68. Journal of Nuclear Materials **420**, 508-518 (2012).
63. Aréna, H., Godon, N., Rébiscoul, D., Frugier, P., Podor, R., Garcès, E., Cabie, M., Mestre, J. P.: Impact of iron and magnesium on glass alteration: Characterization of the secondary phases and determination of their solubility constants. Applied Geochemistry **82**, 119-133 (2017). doi:https://doi.org/10.1016/j.apgeochem.2017.04.010
64. Debure, M., Frugier, P., De Windt, L., Gin, S.: Borosilicate glass alteration driven by magnesium carbonates. Journal of Nuclear Materials **420**(1-3), 347-361 (2012).
65. ANDRA-Collectif: Dossier d'options de sûreté - Partie après fermeture (DOS-AF). In., vol. CG-TE-D-NTE-AMOA-SR2-0000-15-0062, pp. 1-467. ANDRA, (2016)
66. Abrajano, T.A., Jr., Bates, J.K., Mazer, J.J.: Aqueous corrosion of natural and nuclear waste glasses. II. Mechanisms of vapor hydration of nuclear waste glasses. Journal of Non-Crystalline Solids **108**, 269-288 (1989).

67. Abrajano, T., Bates, J.K., Byers, C.D.: Aqueous corrosion of natural and nuclear waste glasses I. Comparative rates of hydration in liquid and vapor environments at elevated temperatures. Journal of Non Crystalline Solids **84**, 251-257 (1986).
68. ANDRA: Projet Cigéo : Revues techniques de préparation à la Demande d'Autorisation de Création (DAC) Revue Finale des Modèles et des Données - première partie (RFMD-1) : Bilan des connaissances phénoménologiques et incertitudes résiduel. In., vol. CG.NT.ADSD.13.0027, pp. 1-269. (2013)
69. Savoye, S., Page, J., Puente, C., Imbert, C., Coelho, D.: New experimental approach for studying diffusion through an intact and unsaturated medium: a case study with Callovo-Oxfordian argillite. Environ Sci Technol **44**(10), 3698-3704 (2010). doi:10.1021/es903738t
70. Savoye, S., Imbert, C., Fayette, A., Coelho, D.: Experimental study on diffusion of tritiated water and anions under variable water-saturation and clay mineral content: comparison with the Callovo-Oxfordian claystones. Geological Society, London, Special Publications **400**(1), 579-588 (2014). doi:10.1144/sp400.9
71. Mualem, Y.: A new model for predicting the hydraulic conductivity of unsaturated porous media. Water Resources Research **12**(3), 513-522 (1976). doi:doi:10.1029/WR012i003p00513
72. Bock, H.e.a.: Self-sealing of Fractures in Argillaceous Formations in the Context of Geological Disposal of Radioactive Waste. (2010).
73. Trotignon, L., Devallois, V., Peycelon, H., Tiffreau, C., Bourbon, X.: Predicting the long term durability of concrete engineered barriers in a geological repository for radioactive waste, vol. 32. (2007)

Appendix

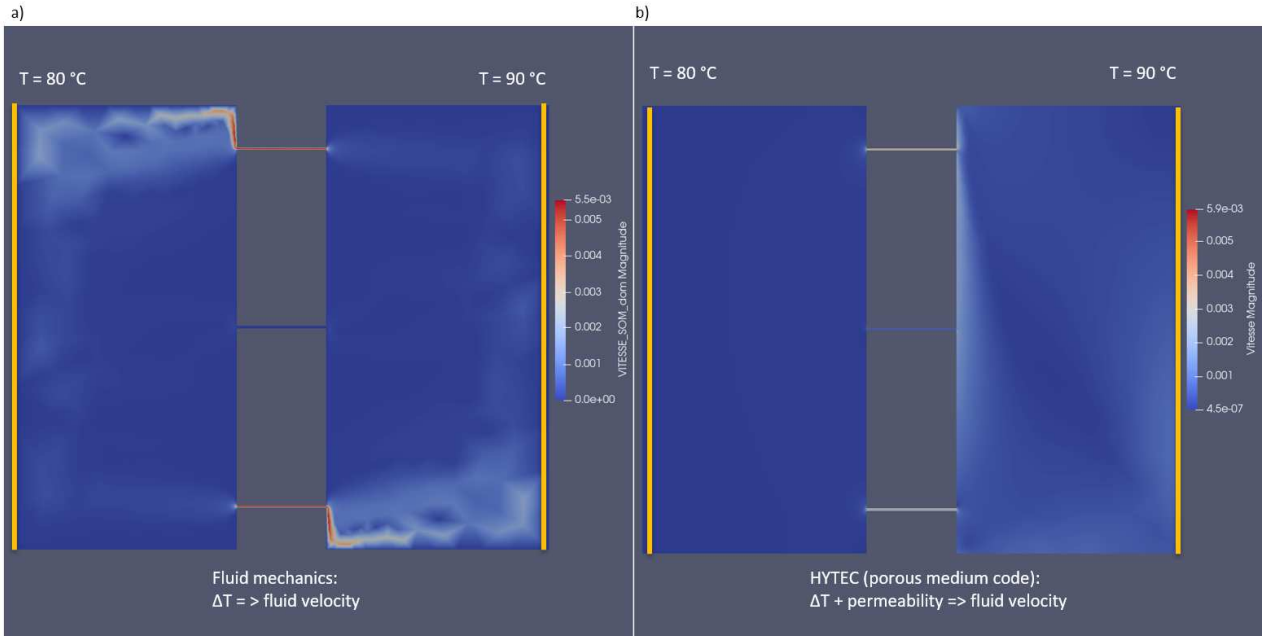

The value of the hydraulic conductivity of the water geochemical unit indicated in Table 3 was set by analogy with the simulation represented in Figure 15. Here three ideal fractures of 1 mm aperture were connected from the right and from the left to two water reservoirs. The objective was to find the value of the hydraulic conductivity of the porous medium (Figure 15b) so that it reproduces the velocity field obtained by computational fluid mechanics modeling (Figure 15a).

Figure 15 Velocity field a) result of the TRIO_U (computational fluid mechanics code) b) result of the HYTEC (porous medium code)

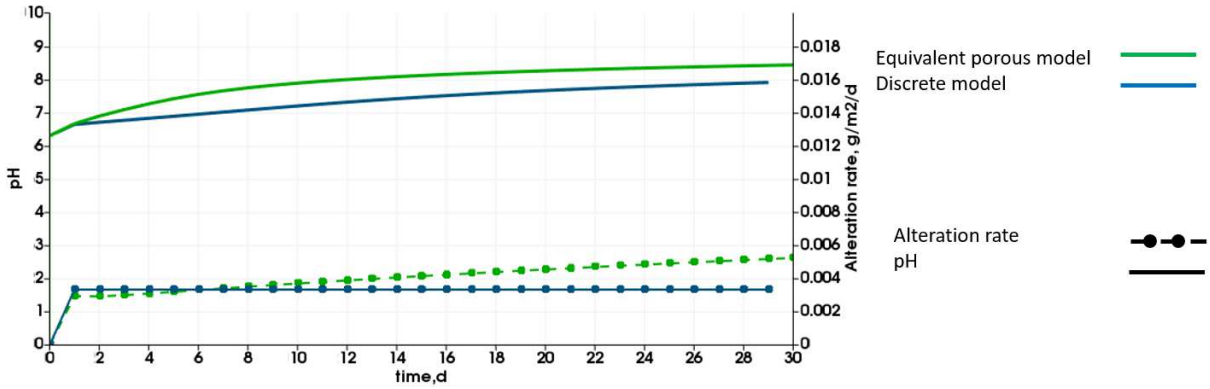

Figure 16 Results of the reactive transport modeling in the case where the impact of the pH and of the affinity term on the glass dissolution rate were not considered: glass alteration rate obtained from boron concentration averaged over the water zones and evolution of the solution pH.

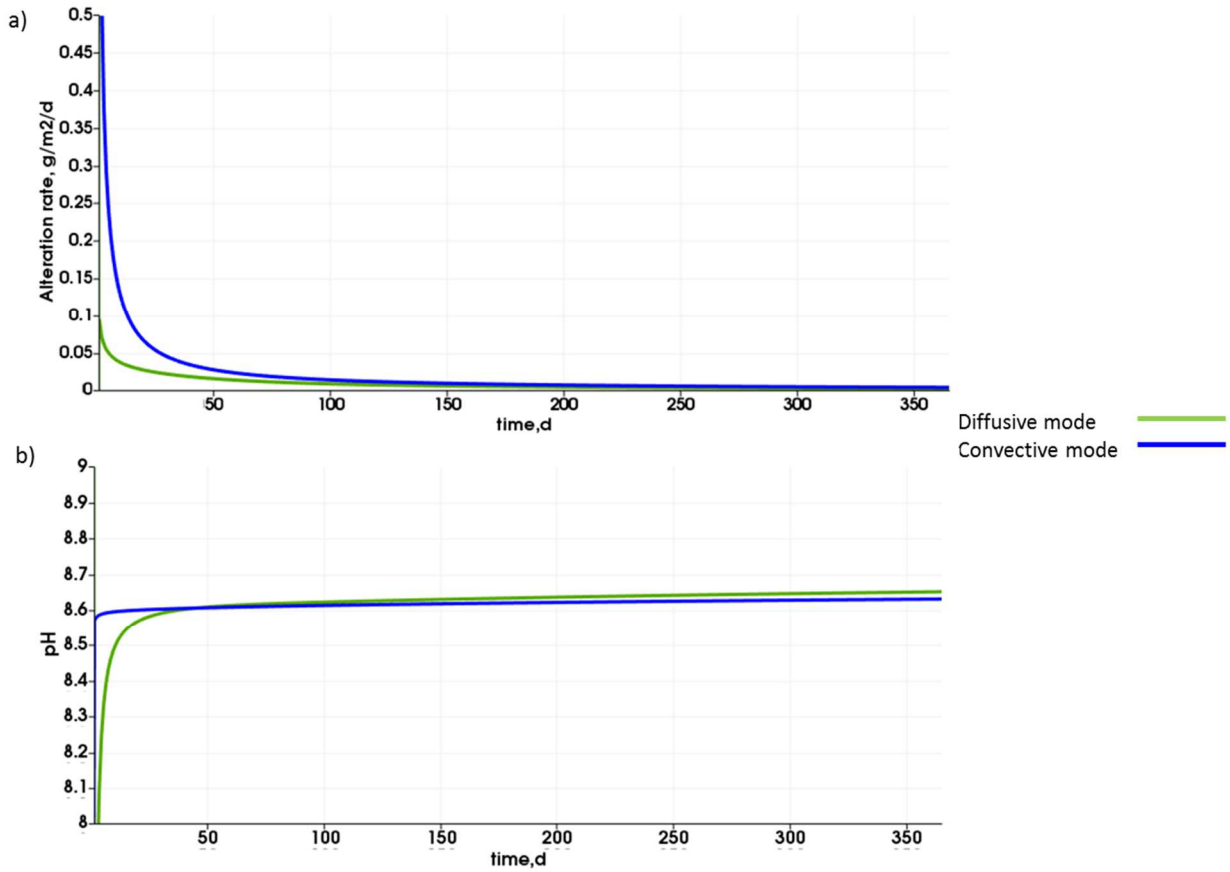

Figure 17 Results of the reactive transport modeling by the equivalent continuum approach in diffusive and convective modes: a) quantity of altered glass obtained from boron concentration averaged over the water zones, b) evolution of the solution pH.

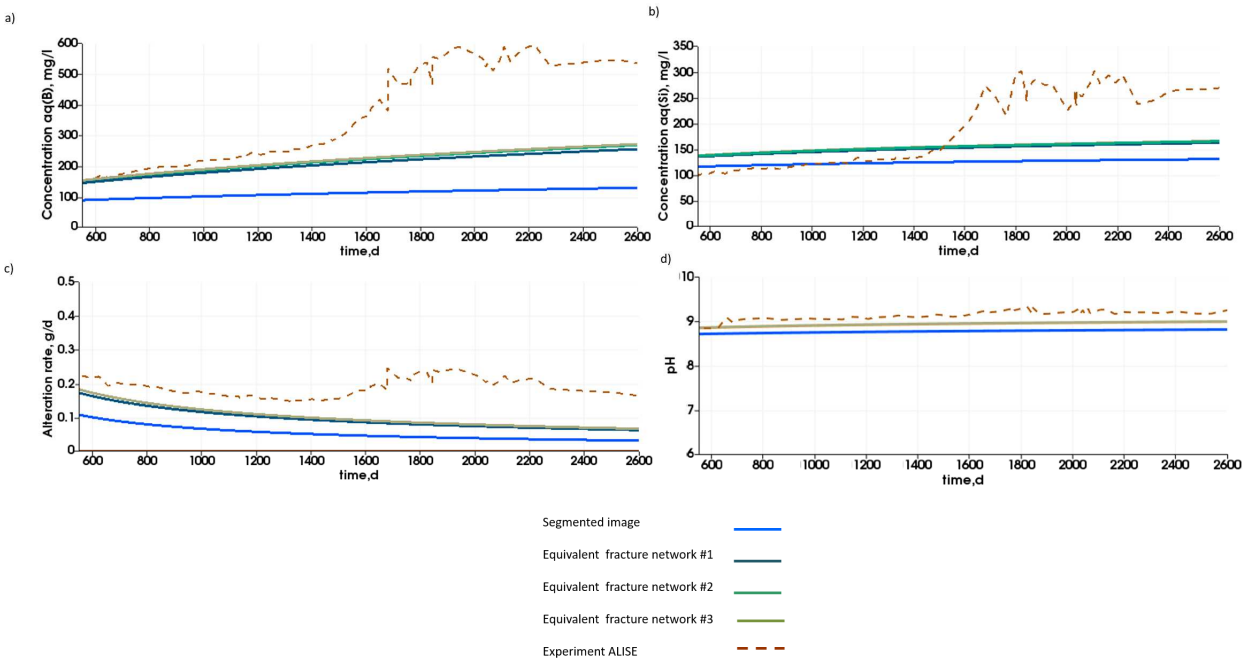

Figure 18 Results of the RTM of the aqueous alteration in the diffusive mode at the scale of the nuclear glass canister: a) average concentration of all aqueous species containing boron present in the solution, b) average concentration of all aqueous species containing silicon present in the solution, c) overall glass alteration rate obtained by total boron release, d) evolution of the solution pH. Experimental results of the ALISE test are documented in [11]. Modelling results do not agree with the experimental results because starting from the 550th day of the alteration the ALISE experiment displays phases of (i) the alteration resumption that is not considered in the applied version of the geochemical model and (ii) the impact of the chemical perturbations due to external interventions.